AN ABSTRACT OF THE THESIS OF

Paul McAlpine Maughan (Name) for the Ph. D. (Degree) in Oceanography (Major)

Date thesis is presented Dec 16, 1965

Title MEASUREMENT OF RADIANT ENERGY OVER A MIXED WATER BODY

Redacted for Privacy

Abstract approved _____ (Major professor)

The results of measurement of solar and long-wave radiation over Yaquina Bay Estuary are reported. The Eppley pyranometer was used to measure solar radiation. A specially designed, wind-oriented, total hemispherical radiometer was used to measure total radiation. The new radiometer has the following characteristics: 1) The radiometer gives an output signal that is independent of the energy fluctuations from non-radiant energy sources. 2) The response of the radiometer is almost totally independent of the wave length of incident radiation. 3) The radiometer is constructed to withstand the corrosive nature of the marine environment. 4) The radiometer is light-weight and compact. It can easily be mounted on a boom for measuring radiant energy from a body of water.

A specially designed data-logging system was used to record the electrical signals from the radiation instruments. The data-logging system integrates, as well as displays, measured radiant

energy. Integrated values of radiation were automatically recorded each hour on paper tape.

Meteorological, oceanographic, and radiation data were recorded continuously during five weeks in June and July, 1965, from the dock at the Marine Science Laboratory near Newport, Oregon. The meteorological and oceanographic data are almost identical to the data reported for the area immediately off the Oregon coast. The measured flux of radiant energy is thus considered to be very nearly representative of the flux of radiant energy in an oceanic environment.

The fluxes of total hemispherical and solar radiation were measured. Average values of incoming and upcoming radiant energy are given. Increasing cloud cover diminished the amount of solar radiation for all solar altitudes. Several established empirical formulae for determining global radiation furnish values within 10% of those measured. The average reflectivity for the period was 0.073.

Incoming long-wave radiation was least for clear skies and increased both with clouds and with vapor pressure. Under overcast skies the incoming long-wave radiation approached the theoretical black-body radiation. The average water surface emissivity was 0.96. There was a daily net loss of long-wave energy from the water surface. None of the empirical formulae tested gave values of effective back radiation within 10% of the measured value.

# MEASUREMENT OF RADIANT ENERGY OVER A MIXED WATER BODY

by

PAUL MCALPINE MAUGHAN

A THESIS

submitted to

OREGON STATE UNIVERSITY

in partial fulfillment of
the requirements for the
degree of

DOCTOR OF PHILOSOPHY

June 1966

APPROVED:

Redacted for Privacy

Professor of Oceanography

In Charge of Major

Redacted for Privacy

Chairman of Department of Oceanography

Redacted for Privacy

Dean of Graduate School

Date thesis is presented December 16, 1965

Typed by Muriel Davis

ACKNOWLEDGMENT

I wish to express my appreciation to Dr. Wayne V. Burt for his assistance in this research.

I am indebted to Mr. Roderick S. Mesecar and Mrs. Susan J. Borden for their contributions to this investigation.

Sincere thanks go to Dr. Herbert C. Curl, Jr., William H. Quinn, and Harold F. Gillis for their suggestions regarding this manuscript.

Finally, special appreciation goes to my wife, Karen, and my children, Jeff, Kim, Julie, and Drew for their encouragement throughout the several years of study.

This investigation was made possible through the financial support of the U. S. Department of the Interior (Educational Grant No. 14-17-0007-132(G)) and the National Science Foundation (Grant No. GP 3548).

TABLE OF CONTENTS

TABLE OF CONTENTS (continued)

LIST OF FIGURES

LIST OF FIGURES (continued)

LIST OF TABLES

# MEASUREMENT OF RADIANT ENERGY OVER A MIXED WATER BODY

## INTRODUCTION

### General Remarks

The primary source of the energy required for continuation of life and functioning of natural phenomena found on the earth is radiant energy. The study of radiation is, therefore, of direct and fundamental importance to many aspects of pure and applied science. A knowledge of both the amount and the distribution of radiant energy is important to such scientists as oceanographers, meteorologists, hydrologists, and engineers.

Of immediate interest to the oceanographer are the dynamic and thermodynamic effects of energy transformations and energy distribution at the air-sea interface. These effects can be thoroughly studied only by combining basic theory with direct observations to derive empirical relationships. Without direct observations to test it, a theoretical model is of little value to the oceanographer.

Notwithstanding future contributions from such sophisticated instruments as the TIROS and NIMBUS satellites, the oceanographer cannot expect the establishment of a large number of oceanic radiation measuring stations in the immediate future. The emphasis must then be to continually improve the present empirical equations

for estimating radiation.

Recently, several of the widely used empirical equations for estimating radiant energy flux over the oceans have been questioned. Laevastu (1960), for example, found large discrepancies among various published formulae for determining reflected radiation. He attributed much of the "scattering of values" to the lack of suitable instrumentation.

Thus, the basic problem is not so much the scarcity of radiation measurements over the oceans, but the lack of proper instrumentation to obtain data of good quality. This thesis offers a partial solution to this problem.

## Object of the Investigation

The primary objective of this investigation was to measure the flux of solar and long-wave radiation in an oceanic environment. It was accomplished in the following way. First, a thorough review of the literature on recent radiation instrumentation was made in order to find an instrument that could measure, with a suitable level of accuracy, solar and/or long-wave radiation in an oceanic environment. The only instrument that met these requirements was the Eppley pyranometer which measures solar radiation only. It was necessary then to design, construct, and test a total hemispherical radiometer to measure solar plus long-wave radiation. The new

radiometer required a special data logging system which was also designed, constructed, and tested. Finally, the complete radiation monitoring system was used to measure the flux of radiant energy over a mixed water body, the climate of which very nearly matched the climate found in an oceanic environment, for a period of five weeks.

The results of the first measurements of long-wave radiation in this area of the Pacific Ocean are reported in this study. This investigation thus acts as a pilot study for further climatological measurements of long-wave radiation.

# DEFINITION OF TERMS

## Classification of Radiation Fluxes

This investigation is concerned only with radiation received on a horizontal surface such as the surface of the ocean. Hence, the term radiation refers to radiation received on a horizontal surface.

### Solar Radiation

Approximately 99% of the sun's radiant energy is contained in the wave length interval 0.15 to 4.0μ (Haltner & Martin, 1957). This electromagnetic radiation is called short-wave or solar radiation. For this investigation solar radiation was sub-divided into three components (Figure 1):

(a) Direct radiation from the sun
(b) Diffuse radiation from the sky
(c) Reflected radiation from the water surface.

The combination of components (a) and (b) is called global radiation; that is, total solar radiation received both directly from the sun and diffusely from the sky.

### Long-wave Radiation

The major portion of the energy radiated by the earth and atmosphere is found in the wave length range 4.0 to 80μ. This

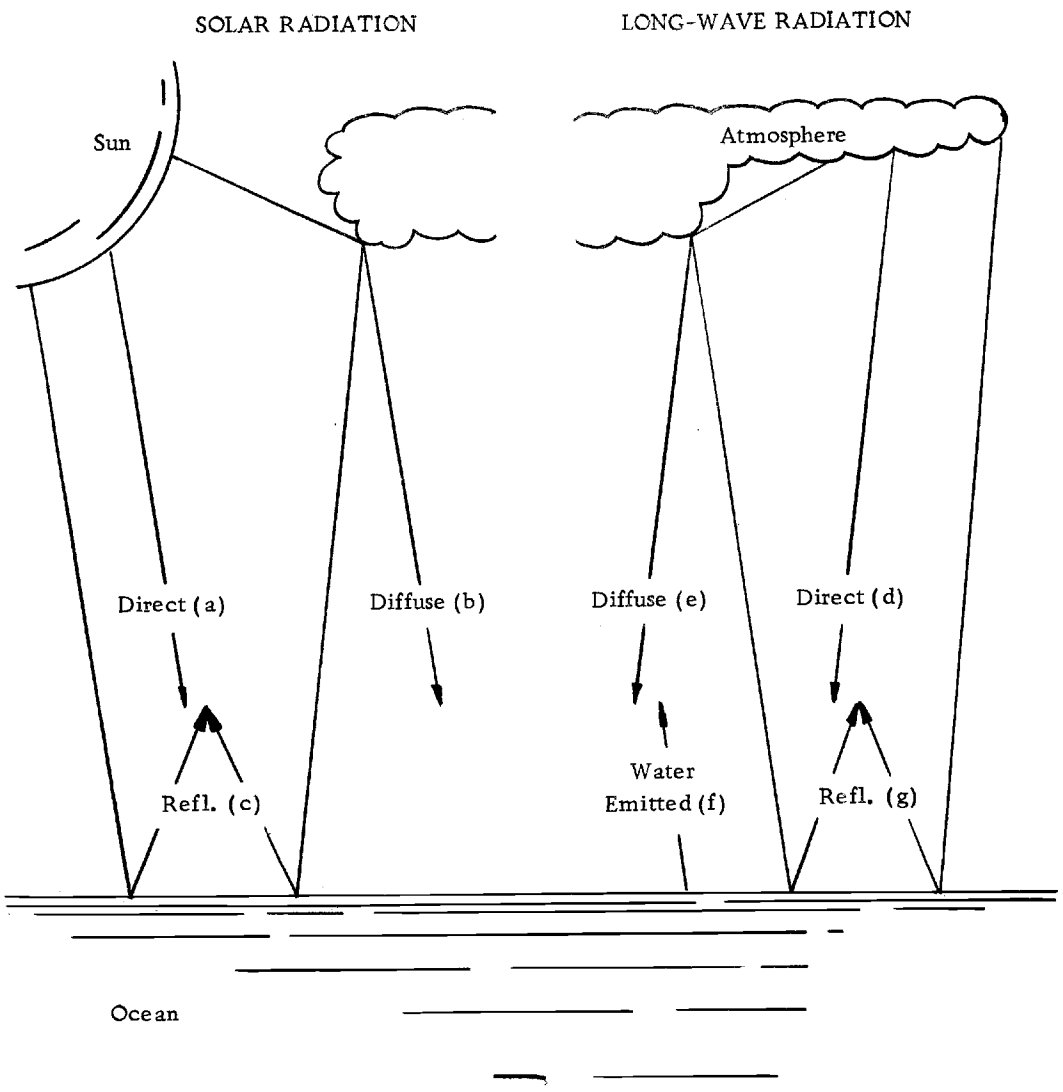


Figure 1. Sources of solar and long-wave radiation. The letters in parentheses are referred to in the text.

electromagnetic radiation is called long-wave radiation. For this investigation, long-wave radiation was sub-divided into four components (Figure 1):

(d) Direct radiation from the atmosphere
(e) Diffuse radiation from the atmosphere
(f) Direct radiation from the water
(g) Reflected radiation from the water surface.

The combination of components (d) and (e) is called incoming long-wave radiation, while the combination of (f) and (g) is called upcoming long-wave radiation (even though the reflected radiation originates from the atmosphere). The difference between incoming and upcoming radiation is called effective back radiation.

## Total Radiation

The components of total radiation were grouped as follows:

(1) Incoming solar plus long-wave radiation (the sum of components (a), (b), (d), and (e) ). Incoming solar plus long-wave radiation is also called incoming total hemispherical radiation.

(2) Upcoming solar plus long-wave radiation (the sum of components (c), (f), and (g) ). Upcoming solar plus long-wave wave radiation is also called upcoming total hemispherical radiation.

The difference between incoming and upcoming total hemispherical radiation is called net radiation.

## Classification of Radiation Instruments

(1) A pyrheliometer is an instrument for measuring the intensity of direct solar radiation at normal incidence. A pyrheliometer used as a secondary instrument scaled by reference to a primary instrument may be called an actinometer.

(2) A pyranometer is an instrument for measuring the solar radiation received from the entire celestial hemisphere. It is suitable for measuring global or sky radiation.

(3) A pyrgeometer is an instrument for measuring long-wave radiation only.

(4) A pyrradiometer is an instrument for measuring both solar and long-wave radiation.

(5) A net radiometer is an instrument for measuring the difference between incoming and upcoming total hemispherical radiation. A net radiometer is also called a balance meter.

# A REVIEW OF RECENT RADIATION INSTRUMENTATION

In the 19th and early 20th centuries Boys, Langley, Coblentz, K. Ångström, Robitzsch, and Abbot developed radiation instrumentation that formed the foundation of radiometry. However, the year 1919 marks the beginning of modern radiometry. In two separate laboratories, Professor Marvin, head of the U. S. Weather Bureau, and Anders Ångström, son of Knut Ångström, designed and constructed instruments that are still used as radiation standards.

The transducer of the Marvin pyrheliometer (Marvin & Kimball, 1926) was a silver disc very similar to that found in Abbot's (1913) silver disc pyrheliometer. A nickel-silver resistance thermometer replaced the mercurial thermometer used by Abbot. With the resistance thermometer, it was possible to measure directly the radiation falling on the disc with a Wheatstone bridge circuit and a sensitive galvanometer. Anders Ångströms's pyrheliometer (1919) was a modification of his father's pyrheliometer. The sensing element of A. Ångström's instrument was composed of four alternately black and white metal strips. Attached to the strips, but electrically insulated from them, were a series of copper-constantan thermocouples. A glass dome was used to cover the entire transducer assembly. The temperature difference caused by the difference in energy absorbed by the hot junctions (black strips) and the cold junctions (white

strips) was a measure of the radiation falling on the transducer.

In 1921, Dorno and A. Ångström (in Kimball & Hobbs, 1923) described a pyranometer using a thermopile for obtaining continuous records of the intensity of global radiation. A year later, Dorno adapted this instrument as a pyrheliometer to measure direct solar radiation only. In both instruments, the output emf of the radiation transducer was so low that the movement of a very sensitive galvanometer needle had to be photographically recorded in order to obtain useful results. In his later paper, Dorno referred to a twelve-element "miniature thermopile" that had a much greater output. Professor Marvin, in 1922, suggested to two U. S. Weather Bureau meteorologists, H. H. Kimball and H. E. Hobbs, that a multiple thermocouple transducer be constructed using Dorno's "miniature thermopile" mounted underlying two concentric metal rings, one white and one black.

Kimball and Hobbs (1923) designed and constructed a pyranometer based on Professor Marvin's suggestions. They built a series thermopile by fusing together 50 thermocouples made from 60% Gold-40% Palladium and 90% Platinum-10% Rhodium wire. This thermopile was then attached to concentric black and white rings cut from copper sheet. A circular bakelite disc was used as a central mounting block which fit inside the inner ring. A second bakelite disc surrounded the outer ring. The base of the central mounting block was

grooved to hold a glass hemisphere 4 1/2-inches in diameter, which surrounded the entire thermopile assembly.

When the pyranometer was exposed to solar radiation, the excess in temperature of the junctions attached to the black ring over those attached to the white ring produced an emf, the magnitude of which was very nearly proportional to the intensity of the solar radiation. Under full sunlight, the thermopile assembly generated about fifteen millivolts.

In the late 1920's, the Eppley Laboratory of Newport, Rhode Island, made several improvements on the instrument without changing its basic design. For example, silver rings 0.01-inch thick were substituted for the copper rings, and the outer bakelite ring was discarded.

The Eppley pyranometer commercially available today incorporates further changes. For example, magnesium oxide and Parsons' Optical Black Lacquer are used to cover the outer and inner rings, respectively. The reflectance of magnesium for wave lengths from the ultraviolet to about 2 $\mu$ is practically constant, and the absorptivity of Parsons' Optical Black Lacquer for the solar wave lengths is very high (see page 33). Thus, the response of the pyranometer may be regarded as independent of the solar spectral energy distribution (Eppley Laboratory, 1964).

A further improvement was made by hermetically sealing the

whole radiation-receiving assembly in a high quality glass bulb. The bulb transmits energy from about 0.28 to 5μ with centers of lower and upper cutoff at approximately 0.30 and 4.5μ, respectively. The transmission is essentially uniform over the range 0.35 to 2.5μ. Before the bulb is sealed to the base, it is carefully heated and exhausted to expel any moisture and then filled with dry air.

The results of laboratory investigations of some of the characteristics of the Eppley pyranometer have been published by Fuquay and Buttner (1957), Latimer (1962), and Karoli, Ångström, and Drummond (1960).

Since the introduction of the Eppley pyranometer, several pyranometers based on the same principles have been constructed. In 1958, Dirmhirm and Sauber (in WMO, 1963) designed a thermopile instrument using black and white segments of the transducer mounted in the form of a star. This instrument is available commercially now in a slightly different form sold under the name of Kahl Star pyranometer or Stern pyranometer. Later, J. L. Monteith (1959) constructed a pyranometer for use in microclimatic studies. He used a miniature Eppley thermopile in his instrument.

In the early 1920's Moll (1923) designed and constructed a unique thermopile for use in radiation instruments. Moll and Gorczynski (Gorczynski, 1924), using the Moll thermopile, constructed a pyranometer by covering the thermopile with two

concentric ground and polished glass hemispherical domes. The domes were sealed into grooves cut into a heavy brass base to which the cold junctions were also attached.

The Linke-Feussner actinometer (in Mõrikofer, 1939) also made use of a Moll thermopile. A thick shell of concentric conical milled rings prevented air currents from affecting the thermopile unit which was mounted at the base, minimized the temperature rise from direct radiational heating, and insured a uniform temperature distribution in the vicinity of the thermopile. This instrument could also be used at night as a pyrgeometer to measure long-wave radiation.

The study of physiological problems prompted Hardy (1934) to design a pyrradiometer with a narrow aperture similar to the Linke-Feussner actinometer. Stoll (1954) redesigned the original instrument and used a flake thermistor to gain added sensitivity and response. The instrument is now commercially manufactured under the name of the Stoll-Hardy radiometer.

The pyrradiometer described by Stern and Schwartzmann (1954) used thallium bromoiodide (KRS-5) to cover the transducer. The cover, nearly transparent to long-wave radiation, reduced the error caused by convective heat transfer from the transducer. The KRS-5 in the shape of a hemisphere covered a 0.0001-inch nickel disc to which was welded a chromel-constantan thermocouple. The top

surface of the disc was gold blackened to absorb the incident radiation. Houghton and Brewer (1954) were able to construct a robust pyrradiometer using a very light electrical resistance thermometer element which was suspended in a vacuum behind a window of KRS-5.

The Schulze radiation balance meter (in IGY, 1958) consisted of two pyranometers, one facing upward and one downward. Each of the two Moll-type thermopiles, connected with opposite polarity, were covered with hemispherical domes of Lupolen-H (polyethylene).

The Georgi Universal Radiometer (pyrradiometer) (in Gates, 1962) was based on the same principle as that of the Schulze radiometer , but was much less complicated. The instrument, provided with an exchangeable hemisphere of polyethylene, could be pointed in any direction to give an instantaneous value of total hemispherical radiation.

V. E. Soumi and P. M. Kuhn (1958) devised a very simple and inexpensive net radiometer of moderate accuracy. The value of the net radiation was obtained by taking the difference of the fourth power of the temperatures of the upper and lower radiating surfaces. The temperatures of the surfaces were read from a mercury bulb thermometer attached to a blackened aluminum sensing element. Two layers of thin polyethylene film over the radiating surfaces kept the conduction and wind losses low. Fritschen and van Wijk (1959) made several improvements on the Soumi-Kuhn net radiometer. For

example, they replaced the mercury bulb thermometer with a thermistor bead to enable electrical readout of the sensing element temperature. The accuracy of the Suomi-Kuhn radiometer has been discussed by Fritschen (1960), Kuhn (1961), Bushnell and Suomi (1961), and Latimer (1962).

J. P. Funk (1959) has described a net radiometer with very thin polyethylene hemispherical domes covering a miniature thermopile transducer. The domes were kept inflated by a pressure pack containing dry nitrogen. A unique heater ring surrounding the transducer assembly prevented the formation of dew on the surface of the polyethylene domes. The accuracy of the Funk net radiometer has been discussed by Latimer (1962).

A shielded, gold-disc radiometer designed for field use has been described by McGuire and Wraight (1960). The pyrradiometer featured a small gold-disc transducer behind a 0.0010-0.0015-inch mica window within a chromium-plated brass enclosure. A second disc, also mounted within the enclosure, was shielded from the window. Two chromel-constantan thermocouples were attached to the two discs with opposite polarity. The radiation received was determined by taking the difference in temperature between the two discs. For radiation measurements greater than five minutes, a water-jacket was used to keep the enclosure at a constant temperature.

Falkenberg (1947) reduced the error caused by convective heat transfer from his net radiometer by rapidly vibrating the transducer. The transducer was attached to a 14-cm steel strip which was vibrated by a motor-driven eccentric. In the net radiometer of Skeib (1953) a "ring" transducer was rapidly rotated by an electric motor. The thermocouple emf was measured by an induction method. The total hemispherical and net radiometers of Dunkle, et al. (1949) and Gier and Dunkle (1951) reduced the error caused by convective heat transfer by directing a steady stream of air over the upper and lower surfaces of the transducer. The transducer consisted of four rows of silver-constantan thermopiles embedded in a 4 1/2" x 4 1/2" flat black plate. Because there was no covering over the transducer, the radiometer is reported to have good spectural response. The Gier and Dunkle radiometers are currently manufactured by Beckman & Whitley, San Carlos, California. The characteristics of the radiometers are further discussed in the IGY Manual (1958), by Karoli, Ångström, and Drummond (1960), and in the Manual of Radiation Observations (U. S. Dept. of Commerce, 1962).

The application of an artificial ventilation source to purge the convective energy equally from both surfaces of a flat-plate transducer has been widely used since it was first introduced by Gier and Dunkle. Concurrent with Gier and Dunkle's work, Courvoisier (1950, in Gates, 1962) developed a vented net radiometer which was similar

in principle but much more elegantly constructed. MacDowall (1955) also followed Gier and Dunkle's design in his net radiometer. The net radiometer described by Suomi, Franssila, and Islitzer (1954) employed a unique vane assembly within the vent tube to control the flow of air over the transducer surfaces. In addition, there was an electric heater element on both sides of the transducer to assist in the control of convective energy.

The Hofman heat-compensated net radiometer (1952, in Gates, 1962) was designed to reduce the error caused by convective heat transfer by using a double faced receiver plate exposed freely in the horizontal plane and without artificial ventilation. A heating current was applied to bring both faces of the plate to exactly the same temperature. Aagard (1958) described what he called a "convection free instrument for measuring infrared radiation." The equivalent blackbody radiation temperature was measured at night by a thermopile embedded in the transducer. A heating current was used to keep the transducer at ambient temperature.

The transducer of the Yanishevskii pyrgeometer (in WMO, 1963) consisted of two thin metal plates whose external surfaces were blackened. The junctions of several thermocouples were bonded to the internal surfaces of the plates. Small copper rods were placed between the junctions of each thermocouple to insure good thermal contact between the upper and lower plate of the pyrgeometer. The

external surface of the lower plate was covered by a metal shield similar to the screen on the Gier and Dunkle total hemispherical radiometer. The temperature difference was then proportional to the radiation balance of the blackened receiving surface. The effects of the wind were accounted for in an empirical heat balance equation written for the blackened receiver; it was necessary to measure the wind velocity over the surface before the absolute values of radiation were known.

B. G. Tunsmore (1962) described a simple radiometer of low accuracy that used large copper plates as the receiving surfaces to insure a long time constant and, thus, low response. No attempt was made to cover or ventilate the transducer.

Lowry (1957) constructed a net radiometer using mercury-in-glass thermometers with a metal plate mounted between their bulbs. The bulb-plate was blackened and served as the receiving surface. Obviously, the sensitivity and accuracy were very poor, but these disadvantages were somewhat offset by the low-cost and portability. Whittier (1964) has described the use of a low-cost silicone cell to measure solar radiation.

Recently, McAlister (1965) constructed a two-wave-length infrared radiometer to measure total heat flow from the air-sea interface at night. This is a specialized instrument for measuring

selective wave lengths. Finite wave lengths can be measured with other pyrradiometers discussed by mounting selective filters over the transducer surface.

# THE DEVELOPMENT OF A TOTAL HEMISPHERICAL RADIOMETER FOR OCEANIC USE

## General Remarks

In the past, most measurements of total hemispherical radiation were made by one of two methods. Prior to the 1940's, a directional radiometer was used to traverse the sky, and the results were graphically or numerically integrated to obtain the total radiation. This method was time consuming and often yielded unreliable results. In 1949, Dunkle, et al. developed a new type of total hemispherical radiometer that allowed the whole sky to be viewed at one time. This instrument recorded instantaneous total radiation, and eliminated the necessity of performing a numerical or graphical integration.

Recently, however, the accuracy of this new type of instrument has been questioned. Kondrat'Yev (1965) states:

> At present the problem of the measurement of thermal radiation fluxes and of the radiation balance is still far from its final solution, although in recent years a number of new designs of pyrgeometers and balance meters have been suggested. Moreover, while the short-wave radiation can be measured with sufficiently high degree of accuracy, the most reliable devices for measuring the thermal radiation fluxes achieve an accuracy which is usually not better than 10-20 percent. The situation is particularly bad in the case of devices for measuring the flux of thermal radiation during daytime.

Dr. A. J. Drummond (1964), Chief Research Physicist of Eppley Laboratory, states that he also has little faith in the commercially available long-wave meteorological radiometers. His impression came from the results of several calibration programs Eppley Laboratory has performed.

Additional problems arise when radiometers are used for oceanic radiation measurements. Elder (1960) says that past attempts to use radiometers at sea have resulted in erratic readings due to "irregular winds" being allowed to strike the transducer. Ashburn (1963) states that the pyrradiometer used at Ocean Weather Station PAPA was not specifically designed for use at sea, and the instrument housing corroded severely. Roll (1965) also reported difficulties from corrosion which caused "electrical faults". Boudreau (1964) was unable to interpret the results from daytime measurements of radiation in the Gulf of Mexico because "... when in sunlight, the fluxes of radiant and thermal energy in the radiometer are large and cannot be assessed to the degree of accuracy required... ".

For the above reasons, a program was set up to design, develop, and construct a radiometer suitable for the measurement of total hemispherical radiation in an oceanic environment.

## Basic Design Factors

All radiometers measure the exchange of energy between a receiving transducer and the target at which they are pointed. In a pyrheliometer or pyranometer, the long-wave-length radiation exchange is between the hemispherical glass cover and the transducer. Because the transducer and glass cover are at essentially the same temperature, the net effect is cancellation of the long-wave-length radiation. The transducer "sees" only the radiation transmitted by the glass cover. Thus, to measure total hemispherical radiation, either an uncovered transducer or a filter that transmits all wave lengths freely must be provided.

The uncovered flat-black transducer, developed by Dunkle, et al. (1949) and selected for use in the new radiometer, is capable of free exchange at all wave lengths. Unfortunately, this type of receiver is subject to other forms of heat exchange, primarily convection, which introduce errors (Maughan & Mesecar, 1965). The IGY Instruction Manual (1958) suggests four methods of eliminating these other forms of heat exchange without affecting the incoming radiant energy.

1. Limit the aperture between the transducer and the radiation source. This procedure isolates the transducer from the natural wind, but is useful only as a standardizing procedure on special occasions.

2. Cover the transducer with a material transparent to long-wave radiation and maintain the cover at the same temperature as the transducer.
3. Introduce a second surface protected in some way from the effect of total hemispherical radiation but exposed to convection, and measure the energy required to maintain it at the same temperature as the fully exposed surface, i. e., an electrical compensation method.
4. Provide artificial ventilation over the transducer surface(s) so that the artificial convective heat loss is much greater than the natural convective heat loss.

All of the above methods of eliminating the effects of convective heat exchange have disadvantages. Limiting the aperture between the transducer and the radiation source also limits the acceptance angle. MacDowall (1955), Bausch and Lomb (Peterson, 1964), Valpey (Lussier, 1964), and Servo Corporation of America (Jerger, 1964), among others, have shown that a material that will transmit only long-wave radiation does not exist. A number of materials transmit effectively in several bands within the infrared region of the spectrum, but no broadband window material is currently available. Any cover will, therefore, be selective. To electrically compensate for the effects of convective heat exchange introduces very difficult problems. The major difficulty in providing artificial ventilation to the

transducer is insuring equal convective heat loss from both top and bottom surfaces of the transducer. All four methods of compensating for the effects of convective heat exchange have been used with varying degrees of success.

Suomi, Franssila, and Islitzer (1954), however, achieved nearly equal convective heat loss from both top and bottom surfaces of their transducer by using a vane within the air stream to control the flow. Also, Courvoisier (1950, in Gates, 1962) used a specially designed wind tube to control the air flow. Thus, by careful design of the artificial ventilation assembly, unwanted forms of heat exchange can be reduced to satisfactory limits. For this reason artificial ventilation was incorporated into the design of the total hemispherical radiometer.

## Description of the Total Hemispherical Radiometer

### The Transducer

#### Theory

Figure 2 shows a multilayered total hemispherical radiation transducer in cross-section. The various heat transfer and temperature terms are indicated. Let the following heat balance equations apply for the steady state conditions:

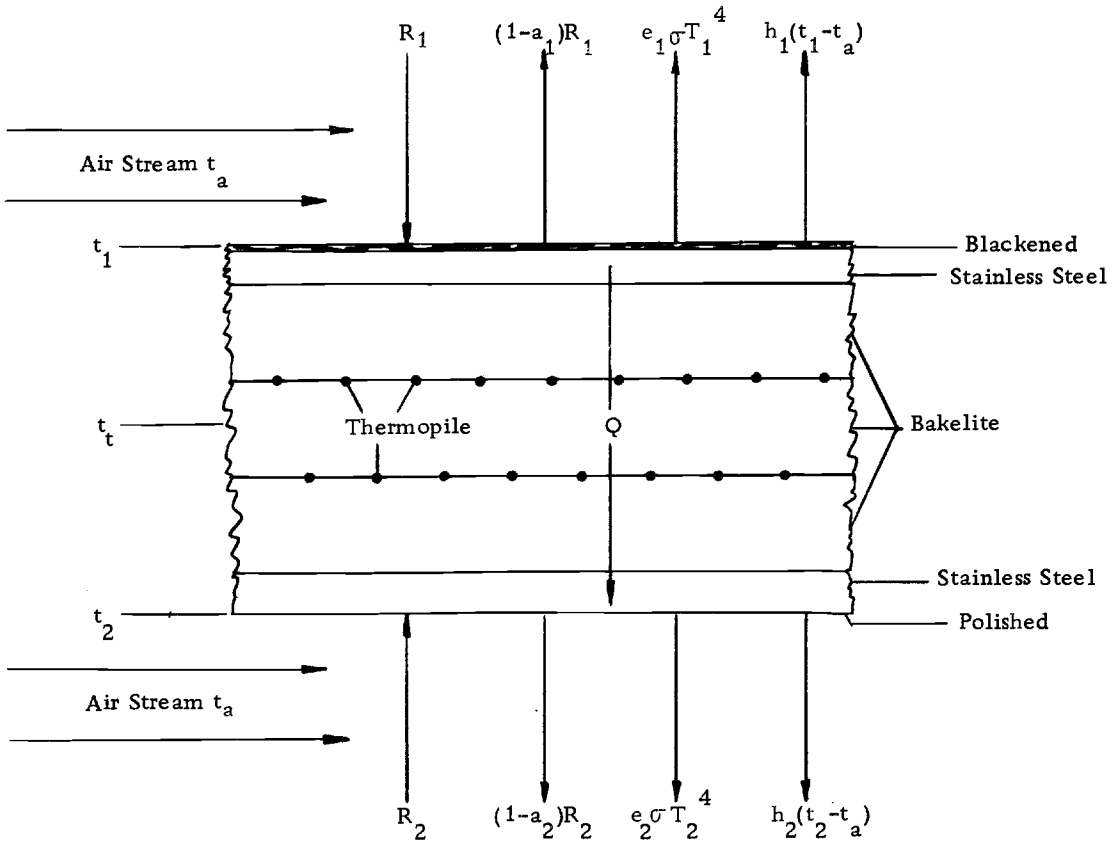


Figure 2. Cross-section of the total hemispherical radiation transducer. The energy terms shown are discussed in the text.

For the top blackened surface

$$R_1 = (1 - a_1)R_1 + e_1\sigma T_1^4 + h_1(t_1 - t_a) + Q \qquad (1)$$

For the bottom polished surface

$$R_2 = (1 - a_2)R_2 + e_2\sigma T_2^4 + h_2(t_2 - t_a) - Q \qquad (2)$$

where

R = Irradiation of the transducer surface, ly/min

a = The absorptivity of the surface, dimensionless

$\sigma$ = Stefan-Boltzmann radiation constant, $0.827 \times 10^{-10}$ ly/min $°K^4$

e = Emissivity of the transducer surface, dimensionless

T = Temperature of the transducer surface, °K

h = Unit thermal convective conductance of the transducer surface, ly/min°C

t = Temperature of the transducer surface, °C

$t_a$ = Temperature of the ambient air, °C

Q = Unit heat flow through the transducer, ly/min

The subscript 1 refers to the blackened surface, and the subscript 2 refers to the polished surface.

Equations (1) and (2) state that the radiation absorbed by the transducer equals the sum of the energy radiated by the transducer, the heat loss by convection from the transducer surface, and the heat conducted through the transducer.

When air is passed over the transducer surfaces, the temperature of the transducer approaches the temperature of the air. If a radiation shield is used to cover the polished surface, the temperature of the air and polished surface can be assumed to be equal. Therefore, $R_2$ is of the same magnitude as $\sigma T_2^4$. Also, $a_2$ and $e_2$ are small and very nearly equal. Thus, with only small error, one can set $a_2R_2$ equal to $e_2\sigma T_2^4$, leaving the heat balance on the polished surface as:

$$h_2(t_2 - t_a) = -Q \tag{3}$$

If the air flows over the top and bottom surfaces of the transducer are equal, then $h_1 = h_2 = h$. If the unit thermal convective conductances of the top and bottom surfaces are different, this difference will be reflected in a change in the calibration constant. Also, the absorptivity of the blackened surface is very nearly equal to the emissivity, i.e., $a_1 \simeq e_1$. Making these substitutions and subtracting equation (3) from equation (1) gives:

$$e_1R_1 = e_1\sigma T_1^4 + h(t_1 - t_2) + 2Q \tag{4}$$

The temperature difference, $t_1 - t_2$, caused by the unit heat flow, Q, through the transducer can be equated through the conduction equation (Boelter, Poppendiek, & Gier, 1944):

$$Q = \frac{k}{L}(t_1 - t_2) \tag{5}$$

where k = thermal conductivity of the bakelite, ly/min °C/cm

L = thickness of the bakelite, cm.

Substituting equation (5) into equation (4) gives:

$$e_1 R_1 = e_1 \sigma T_1^4 + h(t_1 - t_2) + 2\frac{k}{L}(t_1 - t_2) \tag{6}$$

The transducer temperature, $T_t$(°K), is measured halfway through the transducer so that

$$T_1 - T_t = \frac{t_1 - t_2}{2} .$$

Since the difference between $T_1$ and $T_t$ is always very small, the difference between their fourth powers can be approximated by the following expression:

$$T_1^4 - T_2^4 \simeq 4T_t^3 (T_1 - T_M) = 2T_t^3 (t_1 - t_2) \tag{7}$$

Finally, subtracting $e_1 \sigma T_t^4$ from both sides of equation (6), substituting equation (7) into the resulting expression, and dividing through by e, gives an expression for the total radiation:

$$R_1 - \sigma T_t^4 = \left[2\sigma T_t^3 + \frac{h}{e_1} + \frac{2k}{e_1 L}\right] (t_1 - t_2) \tag{8}$$

The voltage, v, generated by the transducer's thermopile is proportional to the total radiation received, or:

$$Kv = \left[2\sigma T_t^3 + \frac{h}{e_1} + \frac{2k}{e_1 L}\right] (t_1 - t_2) \tag{9}$$

where K = calibration constant of the radiometer, ly/min mv

v = transducer output emf, mv

The unit heat flow through the transducer (equation (5) ) can also be expressed as the product of the transducer calibration constant, c, and the transducer output emf:

$$Q = \frac{k}{L} (t_1 - t_2) = cv \tag{10}$$

Hence, the relationship between the transducer calibration constant and the radiometer calibration constant is given by:

$$K = c \left[ 2\frac{L}{k}\sigma T_t^3 + \frac{hL}{e_1 k} + \frac{2}{e_1} \right] \tag{11}$$

Construction Details

In the early development of the radiometer, Dr. H. Poppendiek, Geosciencelimited, Inc. ,assisted in the construction of a radiation transducer similar to the heat flow transducer of Dunkle, et al. (1949). It was desirable to construct a transducer which was as small as possible and had approximately the same output emf as the conventional heat flow meter of Gier and Dunkle (1951). The design selected called for a 2 1/4 " x 2 1/4" transducer incorporating four rows of silver-constantan thermopiles. By placing the thermopiles close together, a more responsive transducer was constructed with a surface area of only one-fourth of that of the conventional heat

flow meter.

Construction details of the transducer are shown in Figure 3. The transducer is constructed from three sheets of 2 1/4" x 2 1/4" x 1/64" black paper base bakelite. Bakelite was chosen because of its ease of fabrication. The bottom plate was notched in four locations along one edge to allow for the attachment of leads to the lugs in the middle plate. The top plate was not altered until after final assembly.

Four 2 1/32" x 13/32" slots were cut in the middle plate to house the thermopile strips. In addition to the slots, small equally spaced indentations were made along one edge to hold the four lead attachment lugs.

The thermopiles were constructed by winding number 40 gauge constantan thermocouple wire around a 2" x 3/8" strip of bakelite until 1 13/16-inches of the strip was covered. The coil winder was set to lay down 80 turns of wire per inch. At that setting, approximately 145 turns of wire were wound on each strip. The thermocouples were made by plating with silver one-half of each strip along the 2-inch dimension.

The electrodeposition plating process forms two lines of silver-constantan thermocouple junctions, the hot junctions on one face, the cold junctions on the opposite face. The thermal conductivity of the wire is considerably higher than the thermal conductivity of the bakelite, but because the cross-sectional area of the

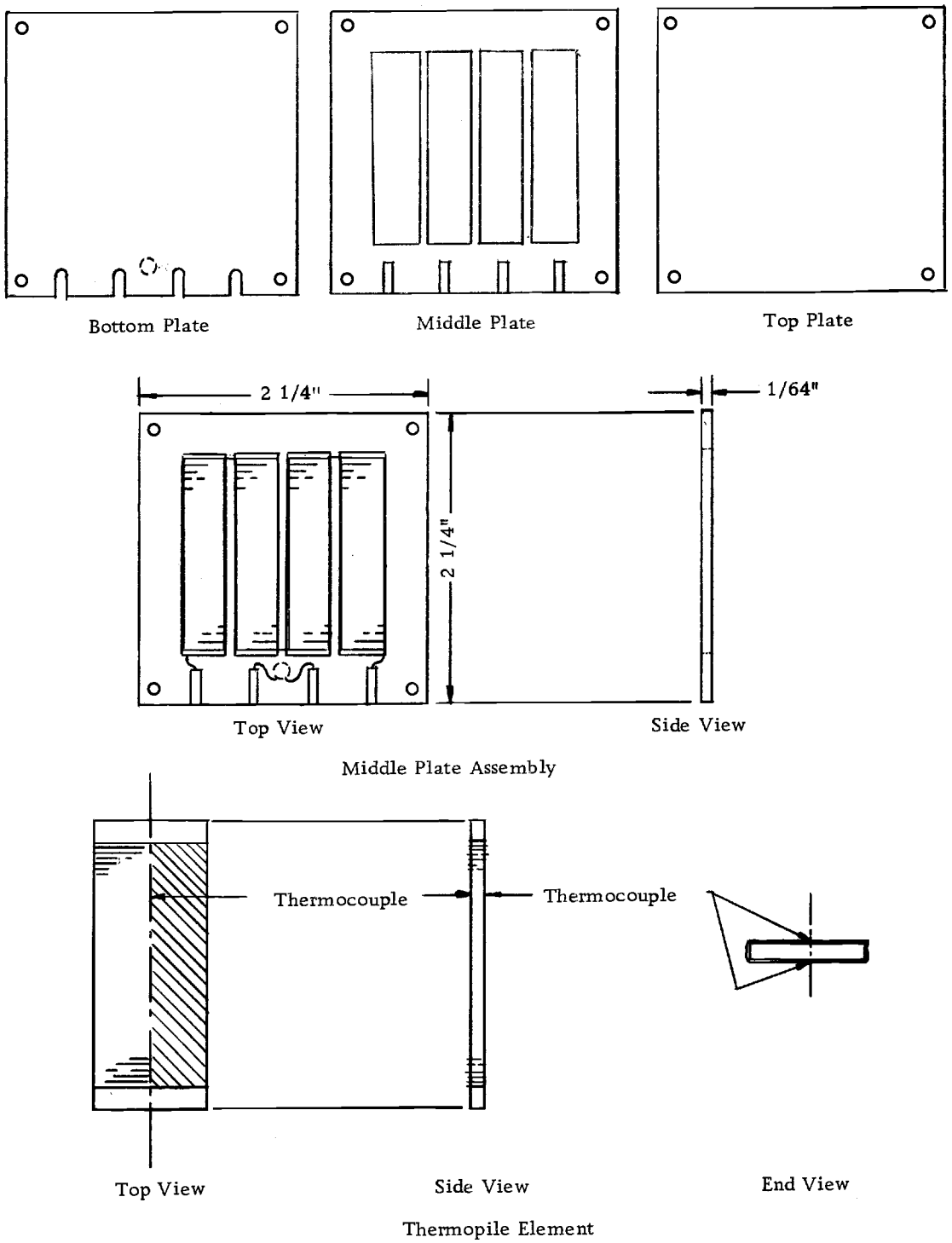


Figure 3. Construction details of the radiation transducer.

bakelite strip, the thermal short-circuit currents are relatively small. Wilson and Epps (1919-1920) have shown that the shunting effect of the constantan core can be neglected because the electrical conductivity of the constantan is much lower than that of the silver. Thus, the silver plating acts as the electrical conductor and makes this type of series thermopile possible.

The temperature of the transducer must be known in order to determine the transducer energy emission term ($\sigma T_t^4$, equation (8)), as well as to correct for changes in material constants at temperatures different from the calibration temperature. For this reason, a precision thermistor (Yellow Springs Instrument part no. 44003) is soldered between the two inner lugs of the middle plate. This thermistor was chosen because its maximum temperature tolerances are held within 0.3 C over the range of temperatures normally found in radiation measurements.

The transducer was assembled as follows. First, the thermopile strips were placed in the slots of the middle plate, and the separate thermopile strips were soldered together in series. The end thermopile strips were then soldered to the outer lugs. After soldering the precision thermistor between the two inner junctions, the entire assembly was bonded together with thermosetting cement.

When used for total hemispherical radiation measurements, the transducer was covered on the top and bottom surfaces with stainless

steel sheeting as shown in Figure 3. Portman (1957) has also used stainless steel plates, 1/32-inch thick, to cover a conventional heat flow meter.

The surface of stainless steel sheet covering the lower surface of the transducer was brightly polished. This polishing reduces the emissivity and absorptivity to the lowest possible values. When the lower transducer surface is also covered by a radiation shield, the small exchange of radiant energy between the lower transducer surface and the radiation shield allows the transducer to be used as a total hemispherical radiometer (Gier and Dunkle, 1951).

The upper surfaces of both the transducer and the shield must be covered with a material of high absorptivity. The absorptivity of the material must be practically the same throughout the whole wave length range of measurement (IGY, 1958). Several covering materials are excellent in the short-wave-length region of the spectrum but are highly unsatisfactory absorbers in the long-wave-length region. Deposits, such as metallic smoke (e. g. platinum, zinc, and gold) and materials such as soot have been used. However, these materials are all very fragile and difficult to use. Therefore, in standard practice, the surfaces are generally blackened with a matte black paint. Gier and Dunkle (1951) used Fuller's Flat Black Decoret paint as a blackening material. This paint had

very good spectral characteristics, but is no longer commercially available.

The IGY Instruction Manual (1958) states that the most suitable absorptive coating so far found is Parsons' Optical Black Lacquer[1]. The National Physical Laboratory, London, determined absorption coefficients for a surface brushed with two coats of this paint. Table 1 shows the results of their findings.

Table 1. Absorption coefficients for Parsons' Optical Black Lacquer (Published in: Eppley Laboratory, 1960)

| Blackbody Temp. | 2580C | 1000C | 200C | Visible |
|---|---|---|---|---|
| Absorption Coef. | 0.985 | 0.980 | 0.985 | 0.985 |

The upper surfaces of both the transducer and radiation shield were covered with this lacquer. One undercoat and two topcoats were spray applied.

Transducer Calibration

A transducer may be calibrated in several ways. One method is to irradiate the transducer with a standard radiation source. Another method, the one used in this investigation, uses a special heat

[1] Manufactured by Thomas Parsons & Sons, Ltd. 70 Grosvenor Street, London, W. 1. England. The Eppley Laboratory, Inc. Newport, R. I. is the U. S. distributor.

flux calibration apparatus. A controlled amount of water is passed through the calibration apparatus and by carefully measuring the incoming and outgoing water temperatures, the heat flow is determined. This known amount of heat is passed through the transducer, and the corresponding thermopile voltage is recorded. The ratio of the heat flow to the thermopile voltage is the transducer calibration constant. The special heat flux calibration apparatus was developed and constructed by Geosciencelimited, Inc., Solona Beach, California. It is designed "... so that end losses and other losses are less than two percent" (Poppendiek, 1965).

In practice, the final calibration constant is determined from the average of many calibration runs. The calibration constants for transducers ME 100 and ME 101 are given in Table 2.

The calibration constant of transducer ME 101 was checked by Geosciencelimited, Inc. at the end of the investigation and was found to be within 2% of the original value.

The material constants change with temperature, so when the transducer is used at temperatures other than the calibration temperature, a correction factor, b, must be used to determine the correct transducer calibration constant. The correction factor is taken from a semi-empirical equation derived by Boelter, Poppendiek, and Gier (1944):

$$b = \frac{0.02186 + 0.0000306\, t_{mo}}{0.02186 + 0.0000306\, t_{m}} \qquad (12)$$

where $t_m$ = the operating temperature of the transducer, °F

$t_{mo}$ = the calibration temperature of the transducer, °F.

Under conditions normally found in the oceanic environment, b ranges from 1.01 to 1.04.

Table 2. Calibration constants for radiation transducers ME 100 and ME 101. The calibration temperature = 80F

| Calibration Run No. | Transducer | |
|---|---|---|
| | ME 100 | ME 101 |
| 1 | 6.52 | 7.36 |
| 2 | 6.56 | 7.34 |
| 3 | 6.55 | 7.34 |
| 4 | 6.52 | 7.32 |
| 5 | 6.53 | 7.33 |
| 6 | 6.52 | 7.33 |
| 7 | 6.54 | 7.28 |
| 8 | 6.55 | 7.33 |
| 9 | 6.58 | 7.34 |
| 10 | 6.55 | 7.33 |
| 11 | 6.55 | 7.33 |
| 12 | 6.50 | 7.25 |
| 13 | 6.53 | 7.32 |
| 14 | 6.61 | 7.32 |
| 15 | 6.49 | 7.29 |
| 16 | 6.50 | 7.29 |
| 17 | 6.51 | 7.30 |
| Average = | 6.54 Btu/hr ft$^2$mv | 7.32 Btu/hr ft$^2$mv |
| = | 0.0295 ly/min mv | 0.0331 ly/min mv |

The Artificial Ventilation

When artificial ventilation is used in a radiometer, it must be sufficient to swamp the effects of the natural wind and heat conduction within the radiometer. If too little artificial ventilation is provided, the radiometer becomes unreliable in very light winds. However, the higher the ventilation rate, the lower the sensitivity. A compromise must be effected (IGY, 1958).

A compromise was achieved by careful selection of the basic components that make up the artificial ventilation assembly: the vent tube, the vent fan, and the air flow controller.

The primary criterion in the vent tube design is that nearly uniform air flow down the tube must be assured. Nearly uniform air flow can be achieved by gradually decreasing the cross-sectional area of the tube between the vent fan and the transducer. Tending to disrupt this flow pattern are the edge effects of the vent tube and the vortices generated at the tips of the blades of a propeller fan.

Hexcel Products, Inc.[2] have described the use of aluminum honeycomb as a means of controlling the flow of air in ducts. Preliminary findings show that a thin piece of honeycomb (about 1/2-inch thickness) placed at the face of a fan increases the downstream velocity as a result of its ability to redirect the air in a

---

[2] Address: 1025 West Arbor Vitae, Inglewood, California.

straight path. Downstream vortices from the propeller fan tips are also greatly reduced (Hexcel Products, Inc., 1959).

A number of applicable types and sizes of vent fans are available. Previously, in radiometers of this type, air was supplied by a squirrel cage fan. However, the motor of a squirrel cage fan is difficult to integrate into the smooth design of a vent tube.

Suitable fans may be selected by use of a term called Specific Speed. Specific Speed is related to three common parameters:

$$Ns = \frac{rpm \times \sqrt{cfm}}{SP^{0.75}} \tag{13}$$

where Ns = Specific Speed

rpm = Shaft speed, revolutions per minute

cfm = Air volume flow, cubic feet per minute

SP = Static pressure, inches of water

For the radiometer vent system under consideration, nominal values are:

$$rpm = 3200$$

$$cfm = 70$$

$$SP \begin{cases} \text{high} = 0.2 \\ \text{low} = 0.1 \end{cases}$$

Substituting these values into equation (13) results in Specific Speeds ranging from 90,000 to 141,000. For this range, vaneaxial and propeller fan are satisfactory.

Several prototypes of artificial ventilation assemblies were constructed and tested with different types and sizes of honeycomb under varying air flows (Figure 6). As a result of these tests, a vent tube 20 inches long tapering from 4 1/2" x 4 1/2" to 3 3/4" x 3/4" was selected. Aluminum honeycomb (1/4-inch cells) was placed immediately in front of the propeller fan. The size of the propeller fan was determined by exposing the transducer to artificial crosswinds of approximately 15-20 knots (generated by a compressed air jet) and observing the output emf of the transducer. When the output emf varied no more than 5% from the no wind case, the air flow was deemed adequate. At this air flow, the air speed across the transducer is approximately 13.5 m/sec.

The final artificial ventilation assembly included a wind vane for directional orientation of the radiometer. The directional orientation idea came from the comments of Dr. Donald J. Portman (1964):

> . . . Whatever your mounting arrangement, I hope you will be able to keep it [the radiometer] oriented so that the natural wind corresponds in direction with the forced ventilation. If not, you may expect 10-15% error and a fluctuating signal under many conditions.

The wind vane offers a simple solution to the problem of maintaining the radiometer so that the forced ventilation corresponds in direction to the natural wind. The natural wind acting on the vane supplies the necessary turning torque to rotate the radiometer in a downwind direction.

Radiometer Construction Details

The body of the radiometer consists of nine components: vent tube, air deflector, wind vane, radiation shield, transducer mounts, vent fan, honeycomb, pivot, and wiring (Figure 4). The vent tube, wind vane, radiation shield, transducer mounts, and air deflector were fabricated from 0.040-inch aluminum sheet. The vent tube has a single seam running the full length of the tube. Before joining this seam, the wind vane was inserted, and the vent tube and wind vane were attached together by aluminum "pop" rivets. All the aluminum parts were anodized for corrosion resistance. The one-hour dip resulted in a moderate gloss finish that can be polished to a higher gloss if desired.

The vent fan was supplied by Rotron Manufacturing Co., and is designated the Gold Seal Muffin Fan. To insure a constant air flow from the fan, the AC power supplied to the fan was regulated.

Hexcel Aluminum honeycomb (Hexcel Al 1/4-.5007-50520 .0007) was inserted in the large end of the vent tube and held by small tabs which had been riveted to the sides of the vent tube.

The pivot was constructed from a standard 1 1/2-inch galvanized "T", machined and tapped to hold two Federal No. 1203LL sealed ball bearings. The pivot was originally designed to house the slip rings necessary to transfer the electrical signals from the

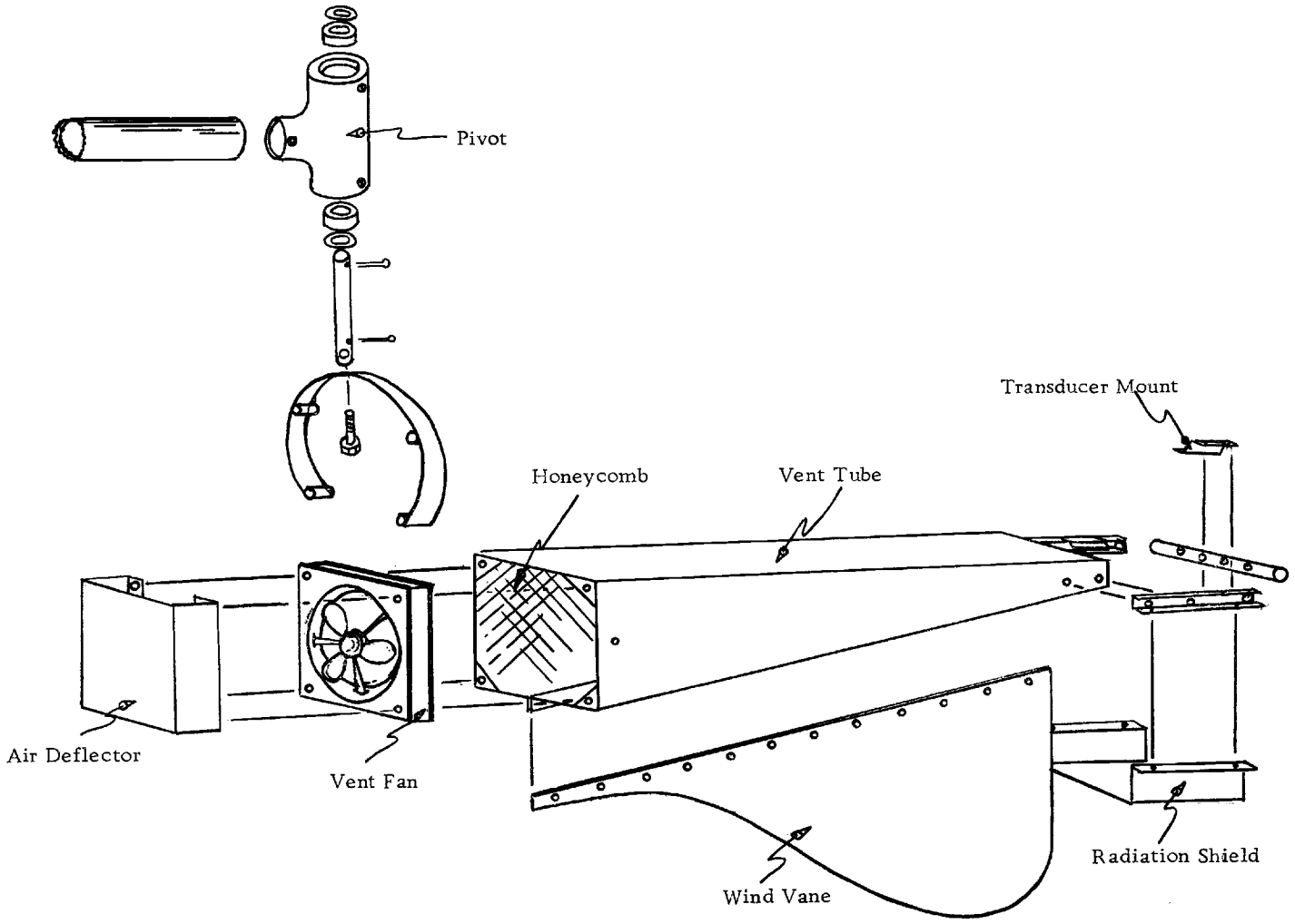


Figure 4. Exploded view of the total hemispherical radiometer. The transducer is not shown.

radiometer to the readout and also supply power to the fan. Cost of slip rings with sufficiently low noise levels almost equaled the cost of the entire radiometer. Observation over several hours of a typical wind vane showed no 360-degree direction changes. Therefore, it was possible to use a straight-through electrical connection.

Six conductor shielded wire was used for supplying power to the fan and bringing the transducer and thermistor output signals to the readout equipment. The completed radiometer is shown in Figure 5.

## Radiometer Calibration

After the transducer has been calibrated and mounted in the body of the radiometer, the calibration constant of the complete radiometer must be determined. The radiometer calibration constant is different from the transducer calibration constant due to the artificial ventilation and transducer surface emissivity coefficients which were not taken into account by the transducer calibration constant. Equation (11) relates the two calibration constants.

A total hemispherical radiometer can be calibrated in three ways. The first method involves using a standard radiation source in a special calibration housing. The second method is similar to the first, but the standard radiation source is replaced by two ideal radiators. The third method involves a direct calibration of the heat

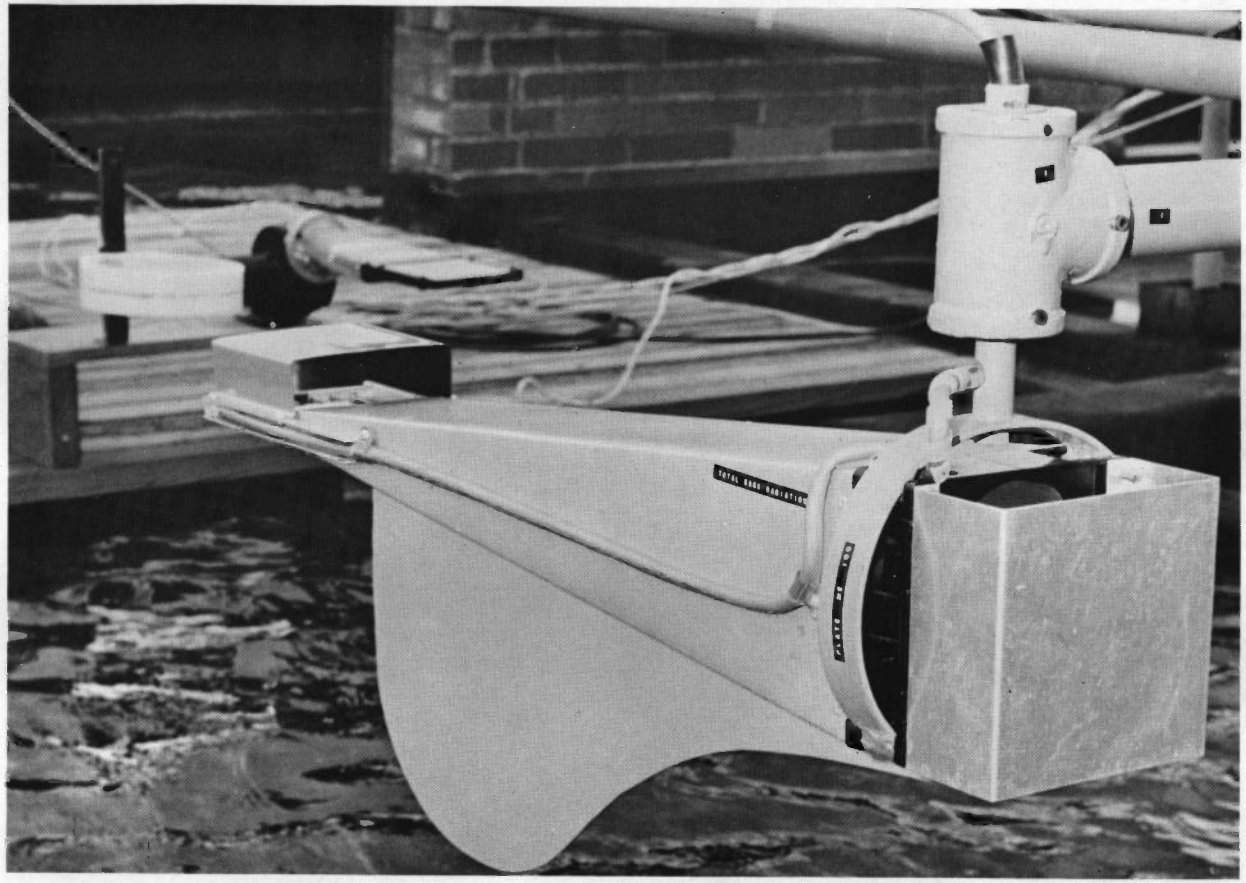

Figure 5. Completed total hemispherical radiometer. In this mounting configuration, the radiation transducer is measuring the upcoming total hemispherical radiation from the underlying body of water.

flux transducer from which the radiometer calibration constant can be determined. Poppendiek (1965) has used methods one and three at the University of California. He reports that "... the [mean] difference between the two methods is approximately 4% ".

Because no standard radiation source was readily available, the third method of determining the calibration constant of the radiometer was chosen. From equation (11), $s = 2\frac{L}{k}\sigma T_t^3 + \frac{hL}{e_1 k} + \frac{2}{e_1}$. For convenience, the English system of units was used to compute the coefficient s. Nominal values of the terms of s are:

$$L = 0.004 \text{ ft}$$

$$k = 0.16 \text{ BTU/hr ft}^2\text{°F/ft}$$

$$\sigma = 1.72 \times 10^{-9} \text{ BTU/hr ft}^2\text{°K}^4$$

$$T_t = 540 \text{ K}$$

$$e_1 = 0.98, \text{ dimensionless}$$

$$h = 9.6 \text{ ft/sec}$$

For these values, $s = 2.258$.

The addition of the stainless steel cover plates over the transducer changes the ratio of L to k by only 0.8 percent. Proof of the small change reflected in the coefficients is shown by determining $L = 0.001$ ft and $k = 10$ BTU/hr ft$^2$°F/ft for the cover plates. Thus, in this example, $s = 2.260$ with the stainless steel covers and 2.258 without the covers.

The radiometer calibration constant is then found by multiplying the transducer calibration constant by the non-dimensional coefficient s. For the two transducers used in this study:

$$K_{ME\ 100} = 0.068 \text{ ly/min mv}$$

$$K_{ME\ 101} = 0.076 \text{ ly/min mv}$$

Table 3 shows the relative magnitudes of the components of s. The radiometer is relatively insensitive to changes in h or $T_t$, but it is highly dependent on the emissivity of the receiving surface.

Table 3. Relative magnitudes of the components of s.

| Expression | Substitution of Values | Magnitude | Percent of Total |
|---|---|---|---|
| $2 \times \frac{L}{k} \sigma T_t^3$ | $2 \times \frac{0.004}{0.16} \times 1.72 \times 10^{-9} \times (540)^3$ | .013 | 0.5 |
| $\frac{h}{e_1} \times \frac{L}{k}$ | $\frac{9.6}{0.98} \times \frac{0.004}{0.16}$ | .245 | 10.8 |
| $\frac{2}{e_1}$ | $\frac{2}{0.98}$ | 2.040 | 88.7 |
| | Total | 2.258 | 100.0 |

## Preliminary Tests

### Wind Tunnel Tests

A laboratory size wind tunnel was constructed, shown in Figure 6, to test the prototypes and final design of the radiometer.

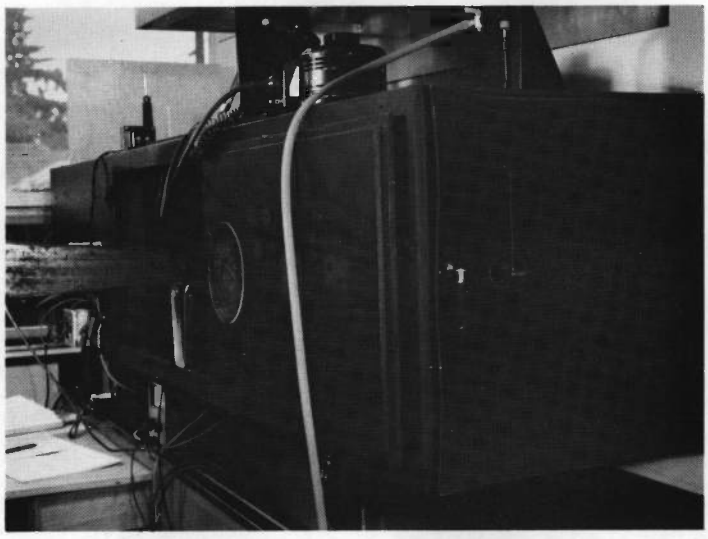

Intake end of wind tunnel showing prototype total hemispherical radiometer in cross-wind test position.

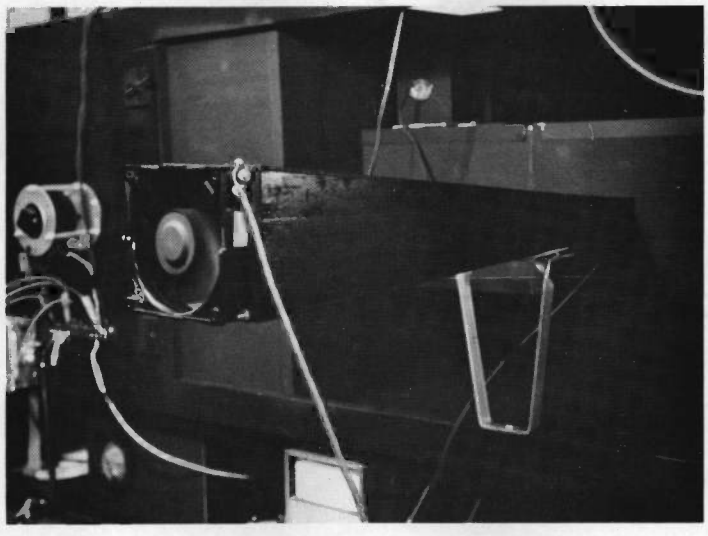

Side view of wind tunnel showing mounting of the prototype total hemispherical radiometer.

Figure 6. Laboratory size wind tunnel used to determine the effects of wind on the new radiometer.

Air is drawn through an effuser (24" x 24" tapering to an 8" x 8" working section) by a four-bladed, 20-inch propeller fan. Wind speeds to 55 knots are controlled by raising a plywood "gate" in front of the fan. A regulated 250 watt projector lamp mounted above the transducer provided a fixed radiant energy level.

Wind speeds were read from a three-cup anemometer placed inside the working section of the wind tunnel. Because it is desirable to know the wind speeds over the transducer surfaces, the anemometer speed was calibrated against two Pitot tubes placed just above and below the transducer surfaces. Each Pitot tube was connected to a micromonometer for the calibration and removed from the duct for the test runs. In this manner, the wind speed over the transducer could be determined simply by reading the anemometer and multiplying by a scale factor.

The wind tunnel tunnel design allowed the entire radiometer to be placed in the duct for downwind tests. For cross-wind tests, the radiometer was placed in a cutout in the side of the working section of the duct.

The results of the wind tunnel tests are shown in Figure 7. It is evident that the minimum percentage change in output (less than 2%) occurs when the radiometer is pointed downwind with the honeycomb and air deflector installed. The effects of the crosswinds diminished as the angle between the axis of the radiometer and the

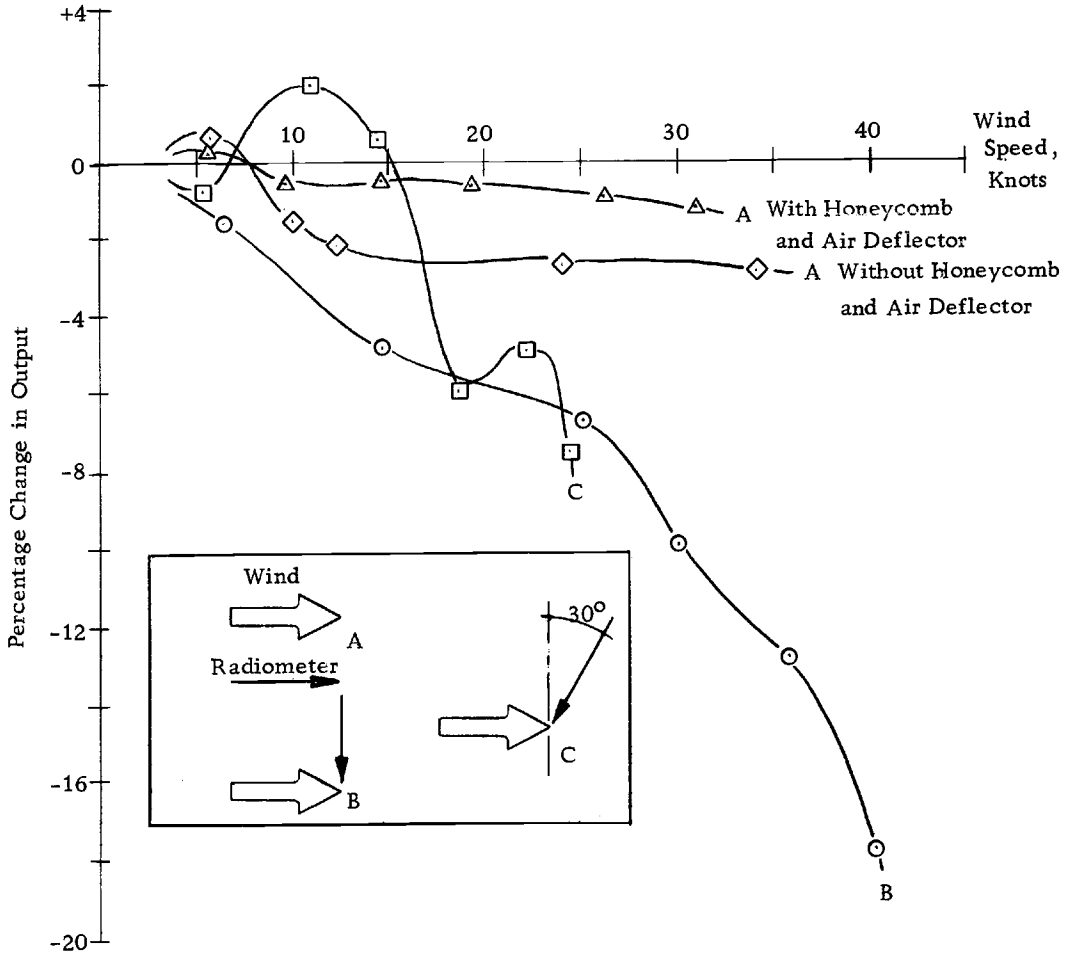


Figure 7. Percentage change in output due to wind on the new total hemispherical radiometer.

direction of the wind decreased. As the radiometer was turned into the wind, the signal changed quite irregularly, depending on the wind speed, but in all cases the maximum deviation was less than that obtained for 90 degree crosswinds. Above 40 knots, vibration and instrument signal noise made readings difficult to interpret.

## Determination of the Radiometer Time Constant

The time constant is defined as the time it takes for the transducer output signal to reach 97% of the total energy level after sudden irradiation. A test box similar to the one described by Johnson (1956) and modified by Fritchen (1960) was constructed to determine the time constant of the total hemispherical radiometer.

The radiometer was placed in the test box (Figure 8) and, after the temperature of the test box had reached approximate ambient temperature, the lamp was turned on. The initial time was noted and the output emf was marked on the millivolt meter each second. In this manner, the time constant was determined to be approximately nine seconds with stainless steel cover plates and approximately five seconds without the cover plates.

## Rooftop Tests

The radiometer was mounted on a boom attached to a specially designed platform on the water-covered rooftop of the Oceanography

Figure 8. Test box with total hemispherical radiometer in position to determine its time constant.

Building at Oregon State University (Figure 9). The primary objective of the rooftop tests was to determine the effectiveness of the wind vane assembly to maintain the radiometer oriented downwind. The most significant results from these tests are as follows:

1. With a wind speed of less than 2 knots, the wind vane assembly was ineffective in maintaining downwind orientation of the radiometer. This was mainly due to bearing friction and the torque exerted by the electrical connecting wire.
2. For wind speeds between 2 and 10 knots, the wind vane assembly maintained the radiometer in the direction of the downwind flow.
3. For wind speeds above 10 knots, the wind vane assembly maintained the radiometer pointed downwind, but fluctuations (at times ± 10-15 degrees) from the "mean flow" were noticed. Possibly the local air turbulence contributed to the rapid back and forth motion.

Downwind orientation of the radiometer has essentially eliminated errors caused by crosswinds. This was shown in several instances during periods of variable gusting winds (10 to 20 knots, occasionally as high as 23 knots) when the radiometer was manually pointed at right angles to the prevailing wind. In this position the transducer output signal was noticeably decreased (at most about

Figure 9. The new total hemispherical radiometers mounted for rooftop tests. On the boom is also mounted an inverted Eppley pyranometer. In the background are the upright Eppley pyranometer (left) and the wind measuring equipment (center).

8%) by the crosswind flow. When the radiometer was released, the signal returned to the original level.

## Summary of Radiometer Characteristics

1. The instrument gives an output signal that is independent of the energy fluctuations in non-radiant energy sources. The capability of the radiometer to be directed downwind has essentially eliminated the undesirable crosswind convective energy that heretofore has been a major source of error in radiant energy measurements without affecting the incoming radiant energy.

2. The response of the instrument is almost totally independent of the wave length of the incident energy (Table 1). The instrument has essentially no windows, filters, or mirrors to selectively absorb radiation.

3. The absorptivity of the blackening material is approximately independent of the angle of incidence of the radiation. Parsons' Optical Black Lacquer has very good properties in this respect (IGY, 1958).

4. The absorbing surface can view very nearly the whole hemisphere.

5. The transducer responds rapidly to changes in radiation. Approximately nine seconds are required for full response; less time is necessary to respond to radiant energy changes normally

found in the oceanic environment.

6. The output emf of the transducer (approximately 33 mv/ly/min) is sufficient for electronic recording and integration.

7. The instrument is constructed of materials that will withstand the corrosive nature of the marine environment.

8. The instrument is rugged enough to withstand frequent handling.

9. The instrument can be mounted on a boom to measure upcoming water-emitted radiation. Because the instrument is lightweight and compact, any inertial effects from mounting the instrument on the end of a boom are minimized.

# THE DEVELOPMENT OF THE DATA LOGGING SYSTEM

## General Remarks

A secondary, but very important, component of a system to measure radiant energy is the data logging system. The low electrical energy levels at which the thermopile type transducer works require rather complicated recording instruments to accurately depict the continuous fluctuations of radiant energy measured by the transducer.

For this investigation, it was decided to continuously record and integrate the output from both the total hemispherical radiometers and the Eppley pyranometers. The data logging system, then, had to provide a continuous display of the radiation parameter measured, an integrated value of this parameter printed at hourly intervals, and, in the case of the total hemispherical radiometers, a continuous display of the transducer temperature.

For continuous records of the radiation parameter, automatic, self-balancing potentiometers are very reliable (World Meteorological Organization, 1963). The primary component of a potentiometric recorder is the null-balance system. Continuously balancing the input signal to minimize the current flow in the transducer is an obvious advantage of this type of recorder. The sophisticated

electronics necessary to bring about this balance, and the resulting high cost, is the major disadvantage of this recorder.

Also suitable for continuous records of the radiation parameter are precision recording microammeters. Unfortunately, ammetric recorders require a continuous flow of current to deflect a stylus. However, if an impedance of sufficiently high resistance is placed in series with the transducer, very small currents will flow. Then, a microammeter can be substituted for a potentiometer. The ammetric recorder has the advantage of being relatively inexpensive.

Radiation data are usually reported as values integrated over half-hourly, hourly, daily, or longer periods of time. These values are often obtained by graphically integrating a curve taken from a strip chart recorder. Schoffer and Suomi (1961), among others, have shown that this method of integration is not completely satisfactory, and is particularly uncertain on partly cloudy days. Minard (1965) states that the most time consuming part of data processing comes in mechanically integrating individual hours of observed records. He concludes that an integrator would improve accuracy as well as eliminate hand integration.

Latimer and Marsh (1962) and Goldwater( 1965) have discussed various types of integrators applicable for use with radiation instruments. In all cases, the integrators are relatively expensive.

Measurement of the transducer temperature requires a

recording Wheatstone bridge circuit, several of which are commercially available, but none of the available circuits was suitable. An electronic readout system of moderate cost was designed and constructed that would meet the requirements of the data logging system. Two prototype readout systems were constructed for use in this investigation.

## Operation of the Readout System

### Integrator

Figure 10 shows a block diagram of the electronic readout system. The integration process is relatively simple. The emf generated by the thermopile in the transducer is passed through an attenuator allowing only a very small current to flow. This signal is then increased by the amplifier and converted to a proportional frequency by the voltage-to-frequency converter. A counter sums the converter output over a specified time period controlled by the program sequence timer. At the conclusion of this time period the timer commands the printer to record the integrated radiation value on paper tape. The offset is used to supply a constant emf to advance the zero count level on the integrator and zero point on the record display. This is used when negative radiation values (i. e. greater transducer emitted energy than incoming radiation) are expected, such as during the night.

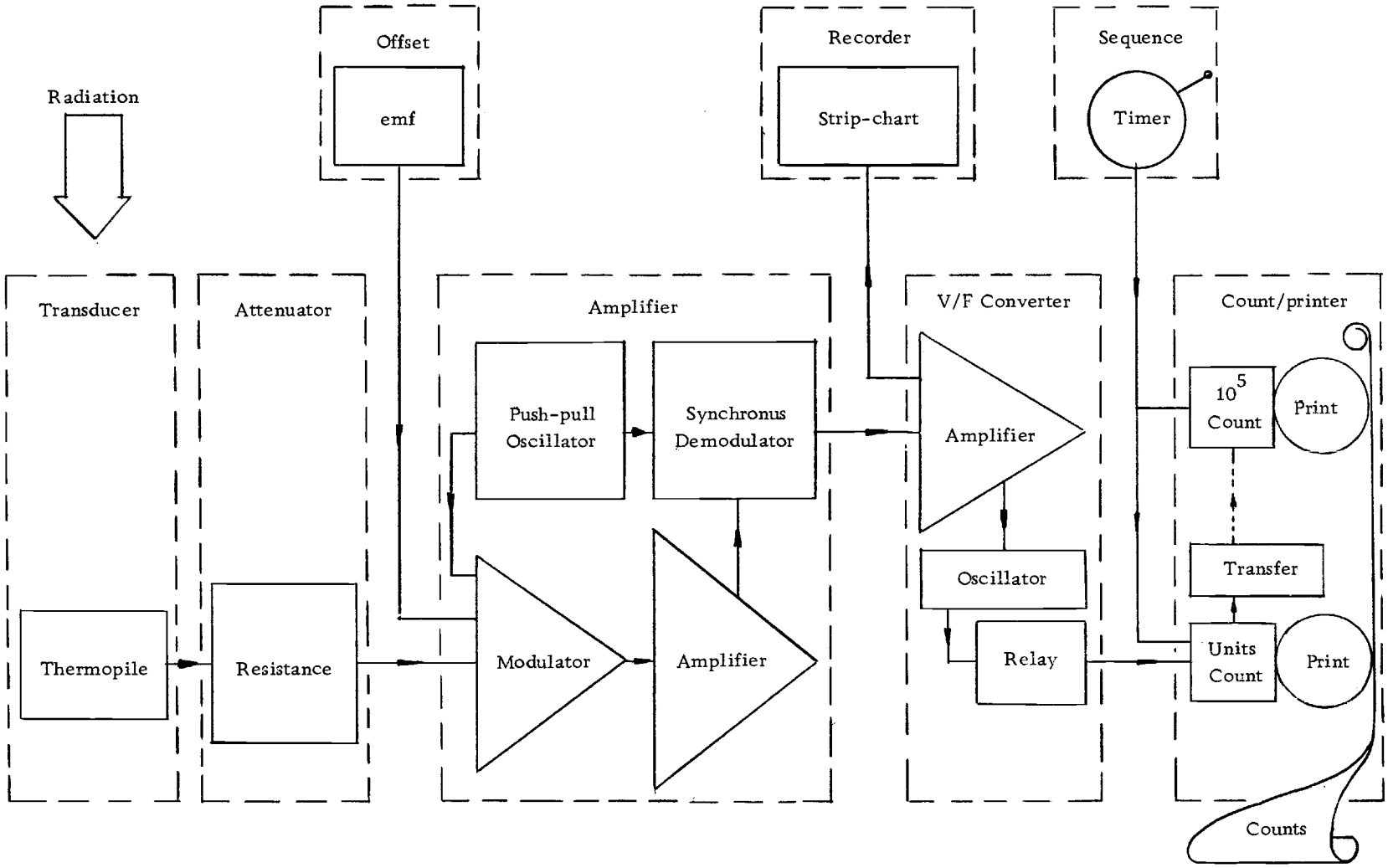


Figure 10. Block diagram of the electronic readout system.

Independent integration channels (Figure 11) were constructed to measure the output signals from two radiation instruments simultaneously. A single program sequence timer controls both channels. Discussion of individual components follows.

Attenuator

Four attenuation modes (10k, 20k, 50k, and 100k ohms) are provided. The mode selection depends on the strength on the incoming signal and the level of amplification set on the amplifier.

Amplifier

Three DC current sensitivity modes are provided (30, 300 and 3000 nanoamperes full scale). The low DC current sensitivity allows an impedance of sufficient resistance to be placed between the transducer and the amplifier in order to insure a very small load on the thermopile. The output voltage supplied to the voltage-to-frequency converter is approximately 100 millivolts full scale. This output voltage is the same on all three sensitivity modes.

Voltage-to-frequency Converter (v/f converter)

The v/f converter was designed by Mr. R. S. Mesecar at Oregon State University. An input of 100 millivolts to the converter generates a frequency of about 30 pulses per second. Provisions are made

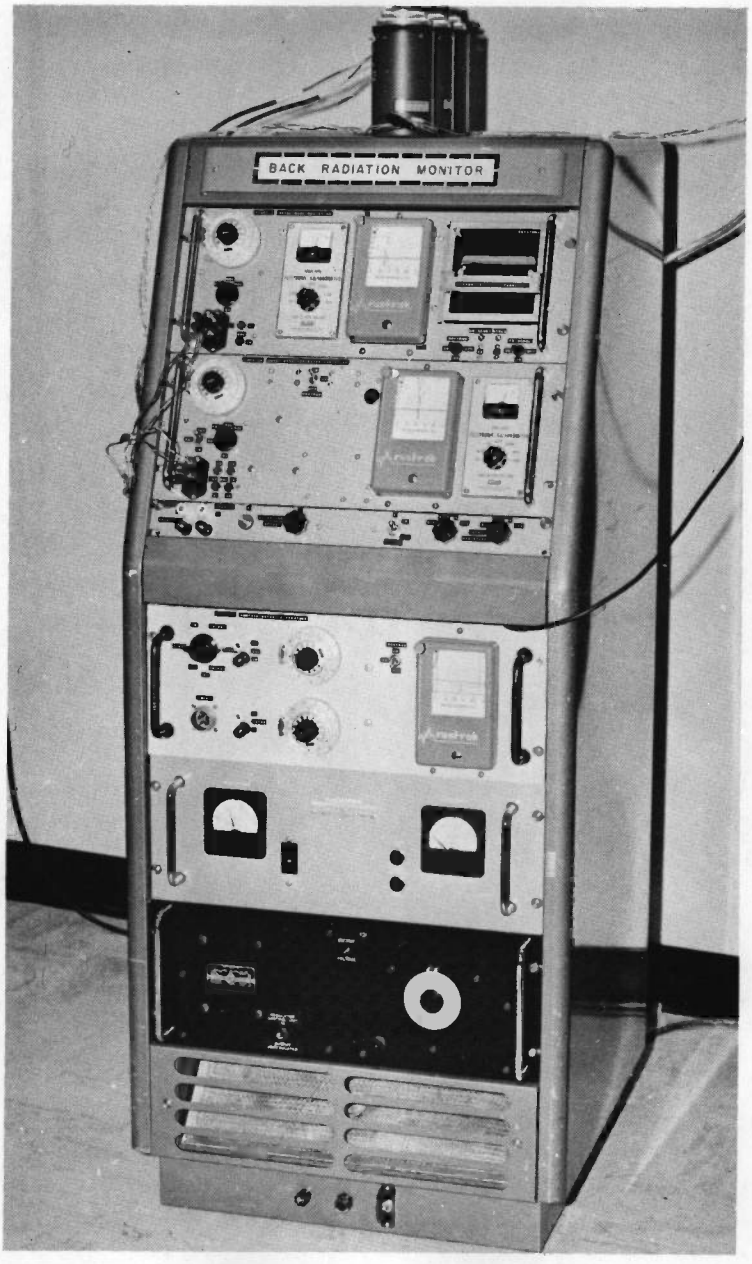


Figure 11. Data logging system used in this investigation. Two integration channels are shown mounted in the upper section of the readout chassis. The surface water temperature and wind speed readout (see Appendix B), regulated DC power supply, and AC voltage regulator are shown mounted in the lower section of the chassis.

in the v/f circuit for calibration of the pulse frequency. The calibration adjustment is relatively simple and can be carried out under field conditions. A circuit diagram of and parts list for the v/f converter are contained in the Appendix.

Counter/printer

Pulses generated by the v/f converter are used to open and close a magnetic relay which supplies a pulse-coded input to the mechanical counting mechanism. The counter, with a $10^5$ total count capacity, sums the converter output for one hour, then prints the total count on a paper tape. After the counter is reset to zero, a new integration sequence begins.

Program Sequence Timer

The program sequence timer supplies two timed switch closures that cause the counter-printer to print the total count on a paper tape and reset the counter to zero. The switch closures are controlled by a cam mechanism driven by an electric clock. At hourly intervals, the cam closes a microswitch which allows current to flow to a magnetic relay. Any time interval can be set by changing the cam. One set of contact closures causes the counter/printer to print, while a second set actuates a relay causing the counter to reset to zero. In this manner, a time delay is imposed on the reset cycle by the serial

closure of the second relay, thus allowing the full print cycle to be completed before reset. Additional contacts of the relay are used to stop the counting coils from advancing during the print cycle. A simple resistance-capacitance circuit controls the contact closure time of the relay.

Temperature Bridge

The transducer temperature is determined by measuring the resistance of a precision thermistor imbedded in the middle plate of the transducer. The temperature readout, shown in block diagram in Figure 12, allows three modes of operation: continuous recording, calibration, and balancing.

Continuous recording is accomplished by measuring the change in resistance by the bridge circuit of the precision thermistor located in the transducer and by using the current caused by the imbalance of the bridge to deflect the stylus of a strip chart recorder. One of the bridge "legs" is set at a resistance of 833.7 ohms, corresponding to a thermistor temperature of 30 C. The recorder reads zero at this temperature. By adjusting the potentiometer between the power supply and the bridge, full scale deflection (50 microamperes) is made to correspond to a thermistor temperature of 0 C.

Calibration is accomplished by replacing the thermistor with a pre-set resistance of 1325.5 ohms. This deflects the recorder needle

to correspond to a temperature of 17.5 C.

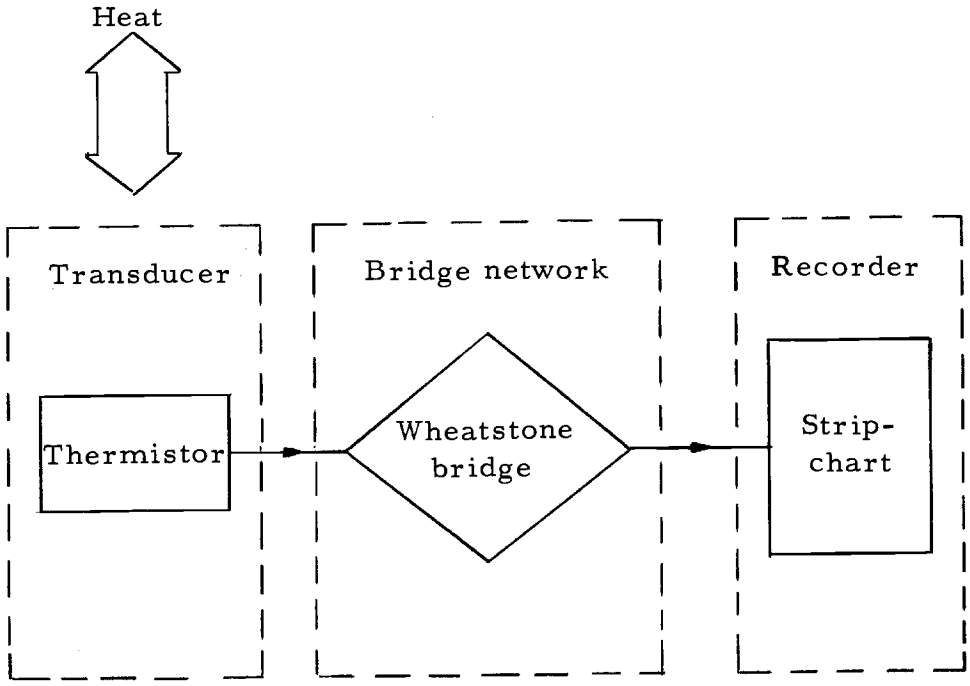


Figure 12. Block diagram of the temperature measuring and recording equipment.

On the balancing mode, the recorder is switched out and replaced by a null balance meter. A variable precision resistor (1%) is also substituted for the 833.7 ohms leg of the bridge. By nulling the signal with the variable resistor, a direct reading of temperature (within ± 0.3 C) is taken. If desired, the electronic galvanometer (amplifier) can be switched out of the integrator circuit and used as the null balance meter.

Record Display

For display of instantaneous values of radiation and continuous recording of transducer temperature, a dual channel strip chart recorder is included. Two independent inputs are synchronously switched internally to permit time sharing of the single galvanometer. A stylus, recording the amplitude of the applied signal, is pressed against the pressure-sensitive paper once every two seconds. The coupling of the primary channel of the recorder to the transducer is shown in Figure 10. Because the recorder is essentially isolated from the transducer through the magnetic modulator, the transducer thermopile does not "see" the load from the recorder. Thus, an inexpensive ammetric recorder can be used conveniently.

The secondary channel of the recorder is coupled directly to the transducer temperature bridge as shown in Figure 12.

## Calibration of the Readout System

Integrator

A block diagram of the calibration equipment is shown in Figure 13. Calibration is accomplished by supplying a known emf to the integrator and reading the resulting count frequency on the oscilloscope. Input emf is varied from 0 to 20 millivolts in steps, depending on the attenuation and operating mode. The common count frequency for

both integrators is fixed by setting the panel meter on the galvanometer/amplifier to 4 nanoamperes. At this setting the v/f converter DC level set is adjusted until the frequency reads 250 milliseconds per cycle or 4 cps.

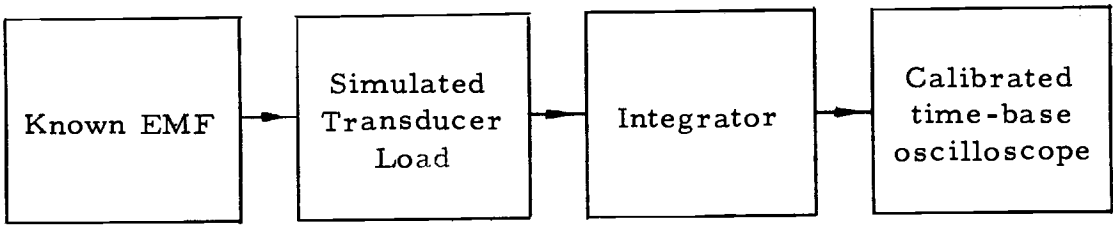


Figure 13. Block diagram of the integrator calibration equipment.

Typical calibration curves are shown in Figure 14. For convenience, curves for both the 30 and 300 na modes are plotted on the same graph. Periodic recalibration of the integrator showed count rates were always within 3% of the original count rate. When the integrator is used with the total hemispherical radiometer, this error amounts to less than 0.06 ly/min.

## Temperature Bridge

The temperature bridge was calibrated by substitution of a precision variable resistor (1%) for the thermistor in the bridge

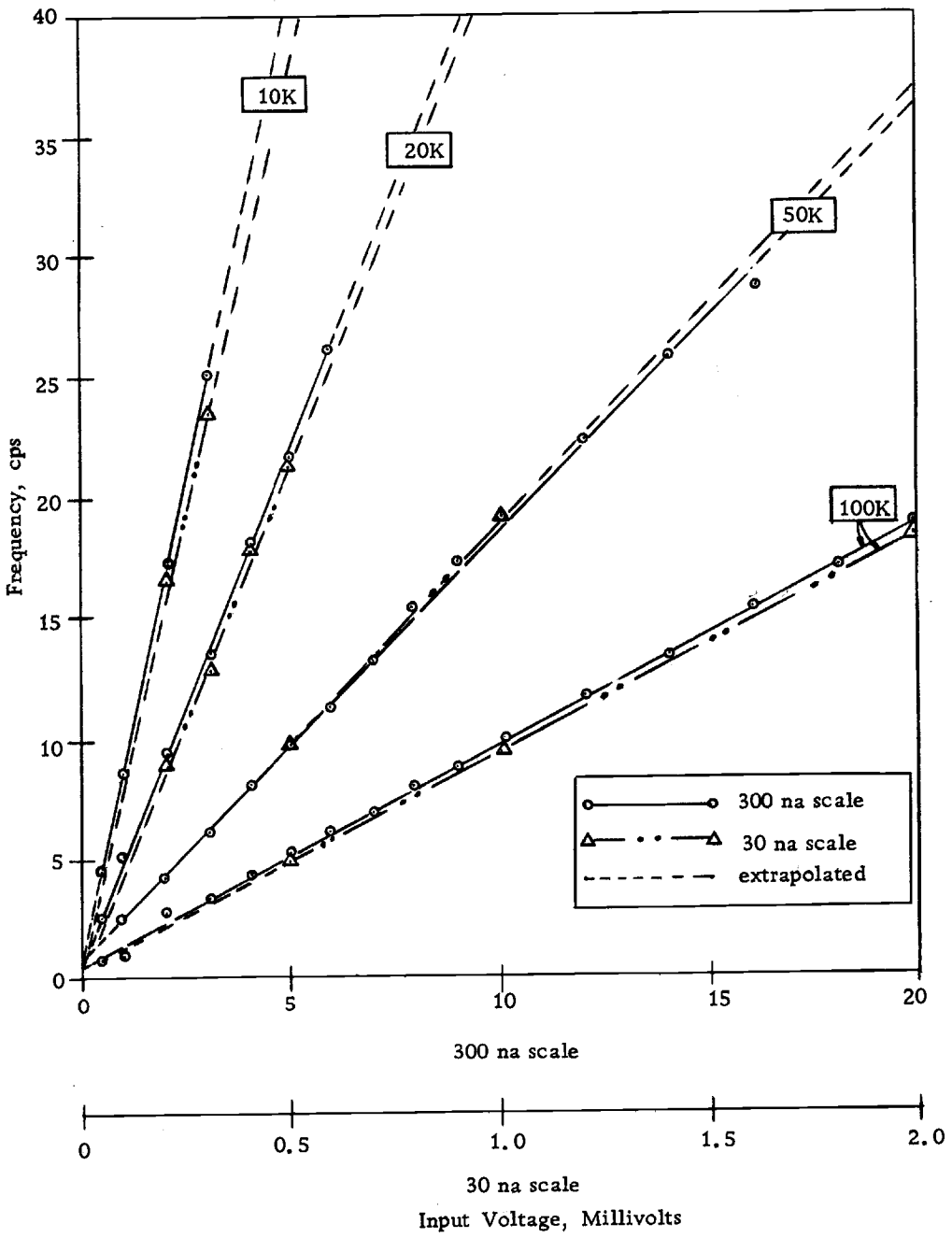


Figure 14. Typical calibration curves for an integrator. The labels 10K, 20K, 50K, and 100K correspond to the resistance setting on the attenuator. The labels 300na and 30na correspond to the mode setting on the amplifier.

circuit and adjustment of the resistor to read the calibrated resistance supplied by the thermistor manufacturer. The thermistor is calibrated to within ± 0. 3 C. Estimates of the temperature can be made on the chart record to within ± 0. 1 C. Therefore, accuracies to within ±0. 4 C are possible. A 0. 4 C change in temperature amounts to approximately a 0. 003 ly/min change in transducer emitted energy or only 0. 7% error in radiation measurements with the total hemispherical radiometer.

# MEASUREMENTS

## General Remarks

For final testing of the system to measure radiant energy in an oceanic environment, the radiation instruments were mounted on the docking facility at the Oregon State University Marine Science Laboratory near Newport, Oregon (Figure 15). In addition, surface water temperature and salinity, wet and dry bulb temperature, vapor pressure, and cloud coverage were recorded. To measure surface water temperature, a specially designed buoy was constructed and attached to the dock (see Appendix B). In situ surface salinity was measured with an Industrial Instruments Portable Salinometer. Arrangements were made to obtain wet and dry bulb temperature, vapor pressure, and cloud coverage data from the U. S. Weather Bureau Airways Observer stationed at the Newport Airport, two miles south-southeast of the Marine Science Laboratory. Whenever possible, the standard three-hourly meteorological observations were supplemented with half-hourly observations made at the dock.

Preliminary examination of the meteorological data (Table 4) indicated very close agreement (with one exception) between these data and the climatic data for the area of the Pacific Ocean immediately off the coast of Oregon. The exception was the mean wind

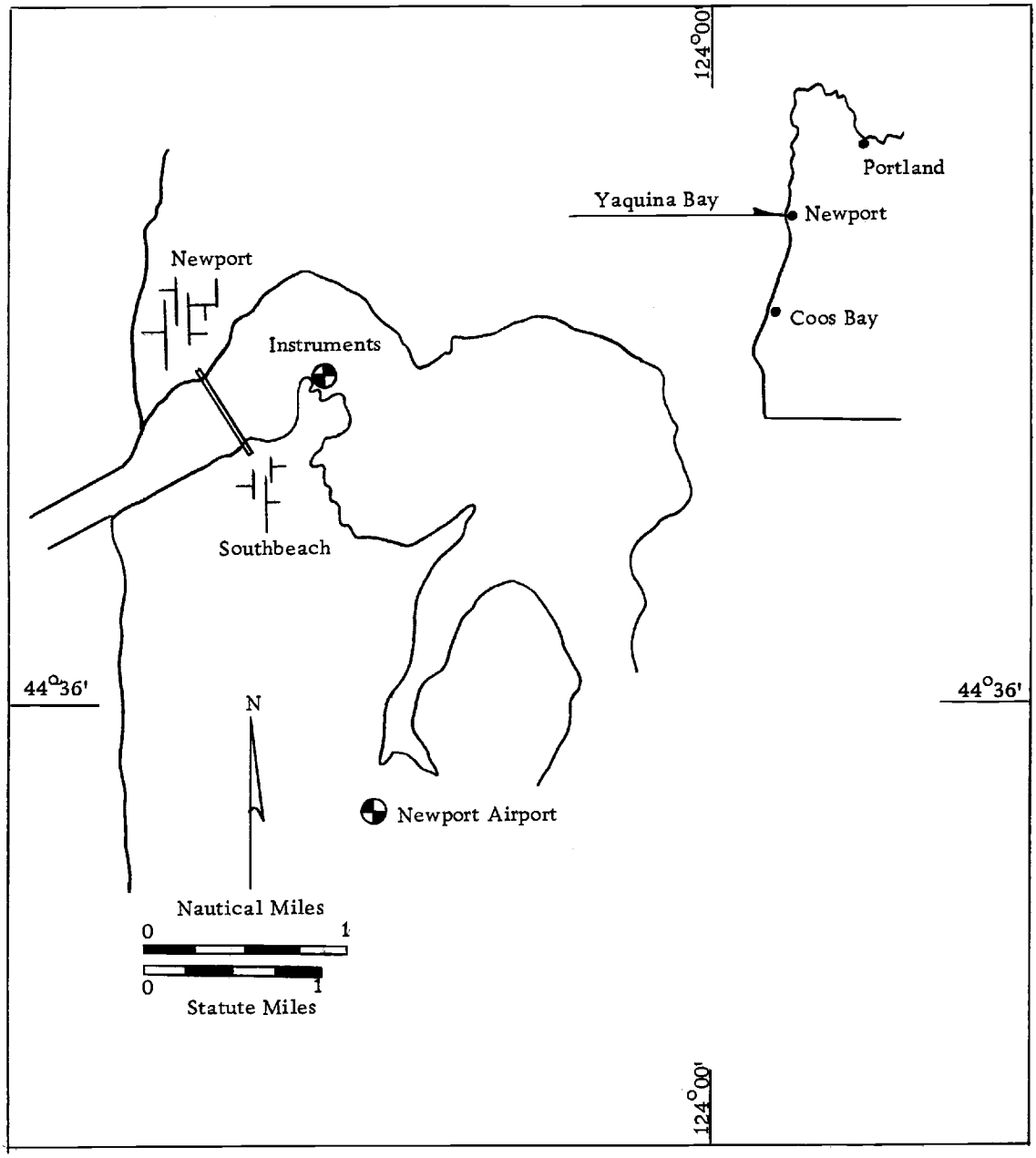


Figure 15. Location of the instruments for measuring radiant energy over a mixed water body. (Base map from Kulm, 1965).

speed. Lane's (1965) mean wind speed of 13.5 knots for June is based on data from ten consecutive years. The mean wind speed of 9.0 knots recorded at the docking facility is based on continuous records taken for 21 consecutive days in June 1965. The primary cause of the 4.5 knot difference is probably due to the local orthographic relief. The northerlies, prevailing during the period of investigation, were restricted from blowing directly on the dock by the presence of a bluff located across the bay, north of the Marine Science Laboratory.

Table 4. Comparison of oceanic and bay climates during the month of June for selected years.

| | Ocean[1] | Newport[3] |
|---|---|---|
| Meteorological Climate | | |
| Mean Air Temp °F | 55.8 | 54.3 |
| Mean Wet Bulb °F | 52.5 | 51.5 |
| Mean Relative Humidity % | 84 | 83 |
| Mean Cloud Cover, tenths | 0.7 | 0.75 |
| Mean Wind Speed, knots | 13.5 | 9.0 |
| Oceanographic Climate | | |
| Mean Surface Water Temp °F | 56 | 52.9 |
| Mean Surface Water Salinity o/oo | 32.07[2] | 31.23 |

[1] Averages given by Lane (1965)

[2] Average from hydrographic reports, Wyatt (1965)

[3] Averages from five weeks of observations near Newport, Oregon 30 May to 2 July, 1965.

The nearness of the docking facility to the ocean results in very nearly identical oceanographic "climates" in the two areas (Table 4). The surface water temperature and salinity are, of course, of primary interest in the study of radiant energy transfer. However, underlying the surface water, there are marked physical differences between the ocean and the bay which do not directly affect the radiant energy flux. These differences led Burt and McAlister (1959) to classify Yaquina Bay Estuary during the month of June as either partly mixed (Pritchard's (1955) class B) or well mixed (Pritchard's (1955) class D).

The nearly identical meteorological and oceanographic climates of the ocean just off the Oregon coast and the Marine Science Laboratory make the latter an ideal place to study the flux of radiant energy in an "oceanic" environment. Therefore, the period of observations from the docking facility was extended and the flux of radiant energy over this mixed water body was considered as very nearly representative of the flux of radiant energy in an oceanic environment.

## The Data

Observations of meteorological, oceanographic, and radiation data were made during a five week period beginning 30 May 1965 and continuing to 2 July 1965. Meteorological observations were made

every three hours (except 0030 and 1830 PST) at the Newport Airport. The wet and dry bulb temperatures observed at the Newport Airport are probably not completely representative of the conditions found at the Marine Science Laboratory because of the inland location of the Airport. Only 18 observations of wet and dry bulb temperature were taken at the Marine Science Laboratory simultaneously with observations at the Newport Airport. However, the available data indicate that the wet and dry bulb temperatures differed an average of only 0.1F and 0.2F respectively between the two sites. Surface water temperature was continuously measured and automatically recorded throughout the period of investigation. Surface water salinity was measured at irregular intervals.

Radiation was recorded every hour throughout the period. Only two readout channels were available to integrate and record data simultaneously. Therefore, only two radiation instruments were "on line" at any one time. The data collected in this manner are summarized in Table 5. Short-interval data were taken during several three-day periods to supplement the regular observations.

The greatest loss of usable radiation data shown in Table 5 resulted from a malfunction of the counter/printer. The count modules were specified to count up to 40 cps, but continuous counts in excess of 15-20 cps caused 4 of the 12 modules to fail. The instrument also failed to reset properly to zero. Almost continuous

Table 5. Radiant energy terms measured at the Marine Science Laboratory dock during selected periods from 30 May to 2 July, 1965

| Observation | Instruments Used With Integrators | | No. Direct Observations | No. Useable | % Useable |
|---|---|---|---|---|---|
| | Integrator I | Integrator II | | | |
| Incoming Global Radiation | Pyranometer[1] | - | 248 | 155 | 62.5 |
| Reflected Global Radiation | - | Pyranometer[2] | 284 | 276 | 97.1 |
| Net Global Radiation | Pyranometer[1] | Pyranometer[2] | 165 | 74 | 44.8 |
| Incoming Total Hemispherical Radiation | Pyrradiometer[1] | - | 271 | 192 | 70.8 |
| Upcoming Total Hemispherical Radiation | - | Pyrradiometer[2] | 336 | 311 | 92.5 |
| Net Radiation | Pyrradiometer[1] | Pyrradiometer[2] | 92 | 23 | 25.0 |
| Incoming Long-wave Radiation | Pyrradiometer[1] | Pyranometer[1] | 305 | 185 | 60.6 |
| Upcoming Long-wave Radiation | Pyranometer[2] | Pyrradiometer[2] | 316 | 311 | 98.5 |
| Effective Back Radiation (Nocturnal only) | Pyrradiometer[1] | Pyrradiometer[2] | 104 | 24 | 23.1 |

[1] The Eppley pyranometer (or the total hemispherical radiometer, i.e. pyrradiometer) was upright.

[2] The pyranometer (or the pyrradiometer) was inverted.

maintenance was required to keep the unit working properly. This problem was eventually overcome by installing a no-reset option. The unit then operated as a continuous serial counter, printing, but not resetting, at each hour.

Whenever the surface of the transducer was wetted by rain, drizzle or mist, the total hemispherical radiation data were lost. The evaporation of moisture from the wet surface cooled the transducer and caused erroneous readings.

## Data Processing and Reduction

All usable radiation records, with the exception of the 0600 and the 2100 PDT observations, were processed. The 0600 PDT radiation values were recorded during the transition period from night to day and the 2100 PDT radiation values were recorded during the transition period from day to night. These records did not show the exact time of sunrise and sunset corresponding to the computed sunrise and sunset given in the American Ephemeris and Nautical Almanac (1963). For purposes of this study the nocturnal time period was defined as the hours between 2100 and 0500 PDT, and the daytime period was defined as the hours between 0600 and 2000 PDT.

The data from the two instruments were recorded on separate channels of the integrator. Each of the total hourly counts was

divided by 3600 to convert the cycles (counts) per hour to cycles per second (cps). This frequency (cps) was used with the calibration curve (Figure 14) to determine the transducer output emf. The resulting energy, in ly/min, was determined by multiplying the transducer output emf by the proper radiometer calibration constant. For the total hemispherical radiometers, the transducer temperature was read from the continuous temperature trace recorded on the strip chart recorder. The average temperature from the previous hour's record was used in the calculation of the transducer-emitted back radiation.

## Results

### General Remarks

The following sign convention will be used throughout the analysis: incoming radiant energy, that is radiant energy from the sun and sky falling on the water surface, will be considered as positive energy; upcoming radiant energy, that is radiant energy reflected and/or emitted by the water surface to the sky, will be considered as negative energy.

### Direct Plus Diffuse Solar Radiation (Global Radiation)

Global radiation makes possible the evolution of life and functioning of most natural phenomena found on earth. For this reason,

a great deal of effort has been centered on the study of global radiation, its distribution over the earth, and its utilization. Numerous direct measurements of global radiation have been made over the continents, and detailed material on the analysis of these measurements is available. However, few direct measurements have been made over the oceans. It is necessary, then, to consider average values which can be either measured directly or computed from empirical formulae based on continental studies.

The measurements made at Yaquina Bay during June, 1965, are the second such measurements taken for purposes of better understanding the distribution of global radiation in Oregon coastal waters. Minard (1965) recently completed an evaluation of global radiation data gathered off the Oregon coast and at Newport, Oregon, in the summer of 1963 . This analysis indicated that the difference in incident global radiation between Newport and the area of the ocean out to 165 miles from the coast was not statistically significant. The average incoming radiation immediately off the coast of Oregon can be accurately estimated from data taken at Newport. Minard measured the hourly radiation at Newport with an Eppley pyranometer mounted on the oceanographic vessel ACONA. The radiation record day was arbitrarily cut off at 0530 and 1830 or 0630 and 1730 [ PDT] , depending upon the length of the day during the four summer months. Integrating Minard's curve of incoming

global radiation (based on an average twelve-hour day) results in an average value of 727.0 ly/day.

For the present investigation, direct global radiation was measured with an Eppley pyranometer mounted upright on the Marine Science Laboratory dock with the instrument leads pointing north, as prescribed by Eppley Laboratories. The average hourly values (Figure 16) increase continually from sunrise until the maximum value of 1.238 ly/min is reached at solar noon. From this point, the values decrease until sunset. The mean value was 676.9 ly/day. This value is 50.1 ly/day (or 8%) less than Minard measured. It is difficult to account for this difference because neither clouds nor weather observations were reported with Minard's radiation data.

The incoming energy from the sun is depleted when passing through the atmosphere, partly through absorption by water vapor and carbon dioxide in the air and partly through scattering against the air molecules or very fine dust. The total effect of absorption and scattering in the atmosphere depends upon the thickness of the air mass through which the sun's rays pass. When the sun is obscured by clouds, the radiation comes from the sky and the clouds. If the sun shines through scattered or broken clouds, the radiation may be greater than from a clear sky, because of the reflection of the clouds (Sverdrup, Johnson, and Fleming, 1942).

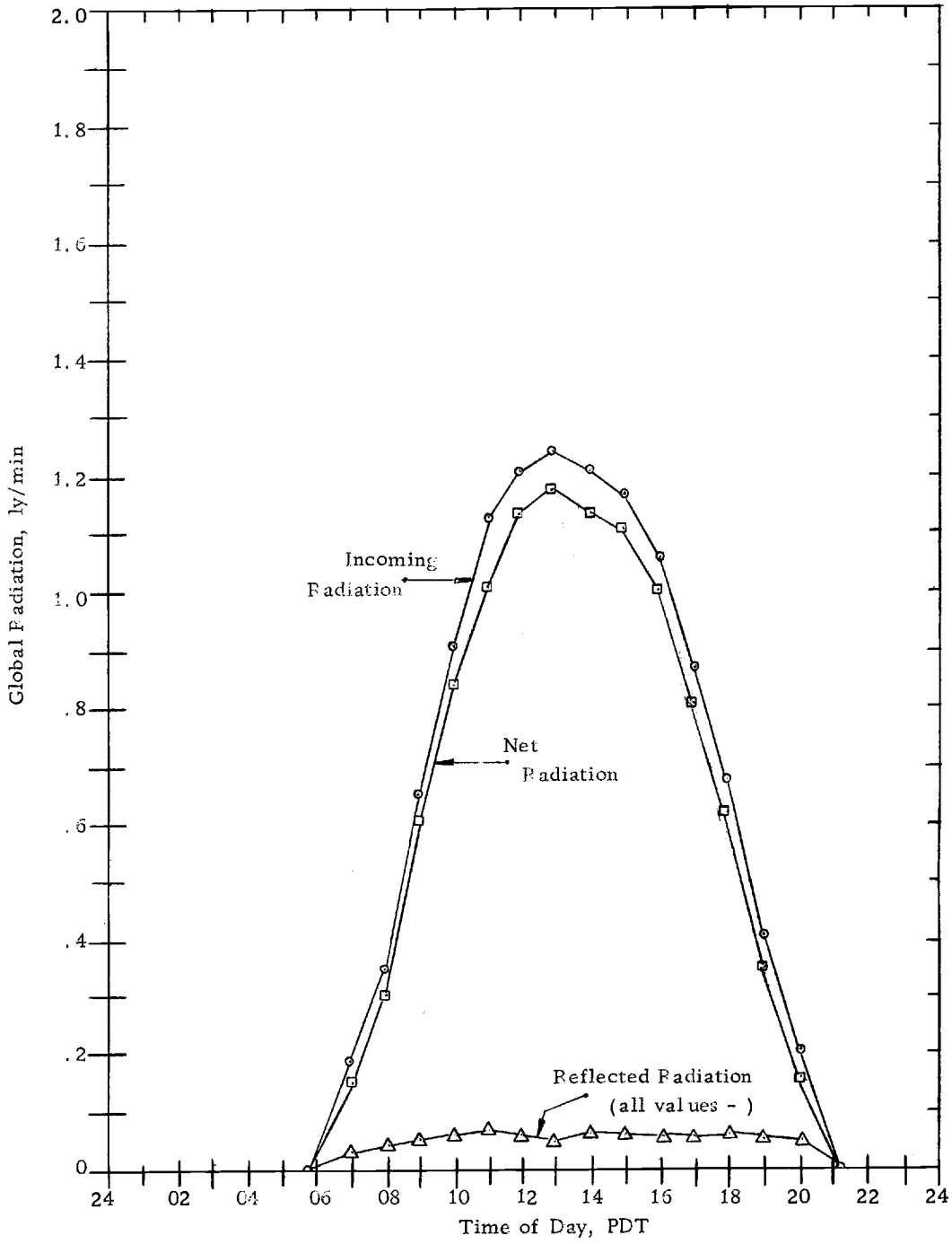


Figure 16. Average global and net global radiation measured at Yaquina Bay, June, 1965.

Figure 17 shows the effects of cloudiness on the incoming global radiation measured at Yaquina Bay. A curvilinear relationship between the incoming radiation and cloud cover is easily seen. S. Fritz (1955, in Raphael, 1962) published curves almost identical to those shown in Figure 17, from a limited number of observations at Washington, D. C., Phoenix, Arizona, and Fresno, California. He observed that although global radiation varied linearly with the percentage of sunshine, it did not vary linearly with cloud cover. Fritz ascribed much of the difference to high cirriform clouds that decrease the percentage of sunshine but tend to reduce global radiation by only small amounts.

The effect of cloudiness on average incoming global radiation has been studied widely by investigators using radiation and meteorological data taken at land based stations. Few studies have been made with data from the oceanic environment. The most recent and notable of the marine studies was performed by Lumb (1964), who derived an empirical relation for incoming short-wave radiation, $Q_s$, at Ocean Weather Station JULIETT, for nine catagories of clouds in the form:

$$Q_s = 135\ s\ (a + bs) \qquad (14)$$

where $a + bs$ is the fraction of solar radiation transmitted through the atmosphere, $s$ is the mean of the sines of the solar altitude

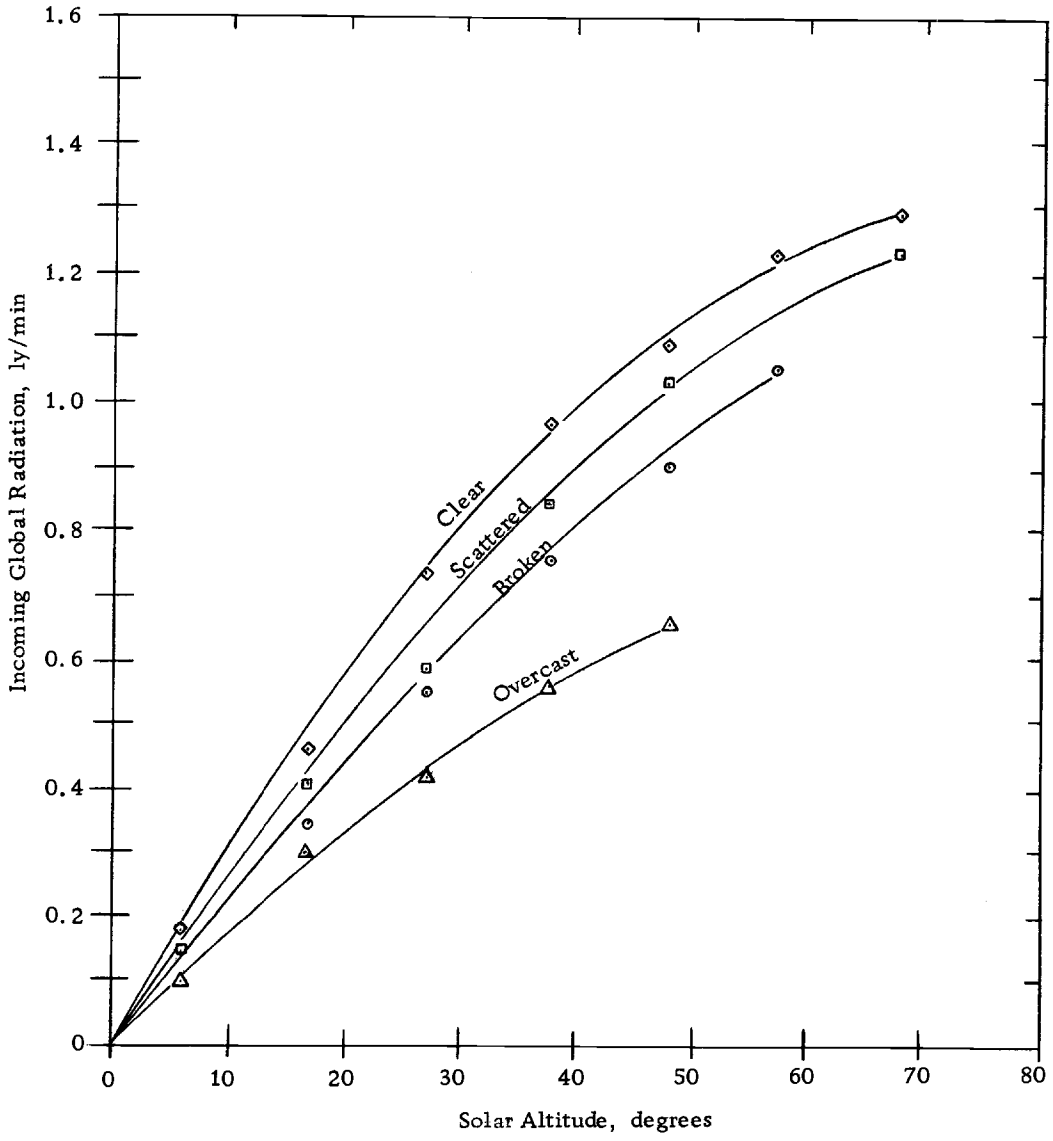


Figure 17. Effect of solar altitude on incoming global radiation for different cloud cover.

at the beginning and end of the hour, and a, b are constants.

Ashburn (1963) derived an empirical formula from records taken over two years at Ocean Weather Station PAPA. His expression is:

$$Q_s = Q_{so} e^{-0.09(1-\cos\pi c)\sec^3 \ell} \qquad (15)$$

where $Q_{so}$ = global radiation with clear skies, ly/day

$c$ = fractional cloud cover

$\ell$ = latitude

Laevastu (1960) proposed the following equation for determining global radiation in a marine environment:

$$Q_s = 0.014\, A_n t_d (1 - 0.0006 c^3) \qquad 16)$$

where $A_n$ = altitude of the sun at noon, degrees

$t_d$ = length of day, minutes

$c$ = cloud cover, tenths

Both $A_n$ and $t_d$ can be found in nautical almanacs.

Roden (1959) used the following empirical equation (Budyko, 1956, in Roden, 1959) in his computation of the incoming global radiation in the California current region of the Pacific Ocean:

$$Q_s = Q_o (1 - k'c) \qquad (17)$$

where $Q_o$ = incoming global radiation with a clear sky, from tables by Budyko

$k'$ = factor depending on latitude, given by Budyko

For his study of the heat budget of the area off the Oregon coast, Lane (1965) adjusted the data taken from direct observations of global radiation at a coastal station. He determined the clear sky radiation at the coastal station from charts prepared by Kimball (1928), then applied a latitude adjustment based on tables by Black (1960). Lane computed a ten-year average value of incoming global radiation for the month of June of 531 ly/day.

Using average meteorological values taken during the investigation, incoming global radiation was computed for Yaquina Bay using equations (14), (15), (16), and (17). The results of these computations (including Lane's and Minard's values) and a comparison between the computed values and the average incoming global radiation measured at Newport during June, 1965 are shown in Table 6.

Table 6. Comparison of incoming global radiation computed from empirical formulae from the authors listed and incoming global radiation value of 677 ly/day measured at Newport, Oregon during June, 1965.

| Equation | Reference | Computed Value ly/day | Difference ly/day | Difference % |
|---|---|---|---|---|
| (14) | Lumb (1964) | 649 | -28 | 4 |
| (15) | Ashburn (1963) | 723 | 46 | 7 |
| (16) | Laevastu (1960) | 670 | - 7 | 1 |
| (17) | Roden (1959) | 393 | -284 | 42 |
| | Lane (1965) | 531 | -146 | 21 |
| | Minard (1965) | 727 | 50 | 8 |

The data in Table 6 indicate that the empirical equations given by Lumb, Ashburn, and Laevastu may be used with short term meteorological data if accuracies of about 10% are acceptable. There is a large difference between the measured value and the value computed from equation (17). The average value from Lane's computations (for a ten-year period) do not agree with our data for 1965. However, for specific years of Lane's data, the agreement is very good. Minard's value has been discussed previously and is shown for comparative purposes only.

Thus, of the several methods for evaluating global radiation in this area of the ocean, Lumb's, Ashburn's, and Laevastu's appear most promising. It is, however, still advisable to measure global radiation directly to obtain the accuracy necessary for application to energy budget studies. Lane (1965) has demonstrated the obvious differences between individual years of meteorological data and their effects on the flux of radiant energy.

## Reflected Global Radiation

Part of the incoming global radiation is reflected from the sea surface, the proportion depending on the altitude of the sun and the condition of the water surface.

Reflected global radiation was measured at selected times throughout the period of investigation with an Eppley pyranometer

mounted upside down on the end of a sixteen-foot boom attached to a corner of the dock at the Marine Science Laboratory (See Figure 9 for mounting arrangement). During high and low tides, the water surface averaged 6 and 16 feet, respectively, below the pyranometer. At average tide conditions, the portion of the dock from which the boom was extended, subtended an angle of about 30 degrees elevation of the pyranometer's view. Unfortunately, the only convenient location on the dock to mount the boom placed the pyranometer in view of a long walkway about 35 feet to the northeast and an access driveway about 40 feet to the southwest. Thus, at all times, the obstructions subtended an angle of about 180 degrees azimuth. However, these obstructions are all more than 16 feet away from the pyranometer. Therefore, the actual elevation angle is much less than 30 degrees, and for this investigation it was assumed to be 15 degrees. For isotropic radiation the fraction of the total flux intercepted by an obstruction is $(1 - \cos 2\delta)\phi/4$ where $\delta$ is the elevation and $\phi$ the azimuthal angle subtended. For the dock obstructions, this fraction is about 10%.

Because the boom was mounted from the northwest section of dock, the inverted pyranometer was in an early morning shadow from the sun. During the entire investigation shadows were visible from sunrise until approximately 1000 PDT. Thus, no reflected shortwave radiation directly from the sun was recorded until nearly

mid-morning. The effect of blocking the sun's energy from the water surface is evident upon examination of Figure 16. After sunrise the reflected diffuse short-wave radiation increased slowly, rather than rapidly as expected, until mid-morning. At about 1100 PDT, when the sun's elevation was about 58 degrees, the reflected global radiation decreased to a minimum 0.057 ly/min, then increased slightly. Little change was measured thereafter until a rapid decrease occurred just before sunset. The average value of reflected global radiation was -45.7 ly/day. If the early morning values were adjusted to match the late afternoon values, taking into account the blocking of the sun's reflections, the average value would be -49.5 ly/day.

Lane (1965) computed reflected global radiation for his heat budget analysis off the Oregon coast. His average value for June of -29 ly/day is only 63% of the value measured during June 1965.

The average value of reflected global radiation measured at Yaquina Bay is consistent with that computed by multiplying widely accepted values of reflectivity by incoming global radiation. Raphael (1962), using data from E.R. Anderson's Lake Hefner study (1954), published a curve of average surface water reflectivity for conditions of low and high clouds as a function of solar altitude (Figure 18). Curves of average reflectivity for all cloud conditions at Yaquina Bay agree closely with Raphael's curves.

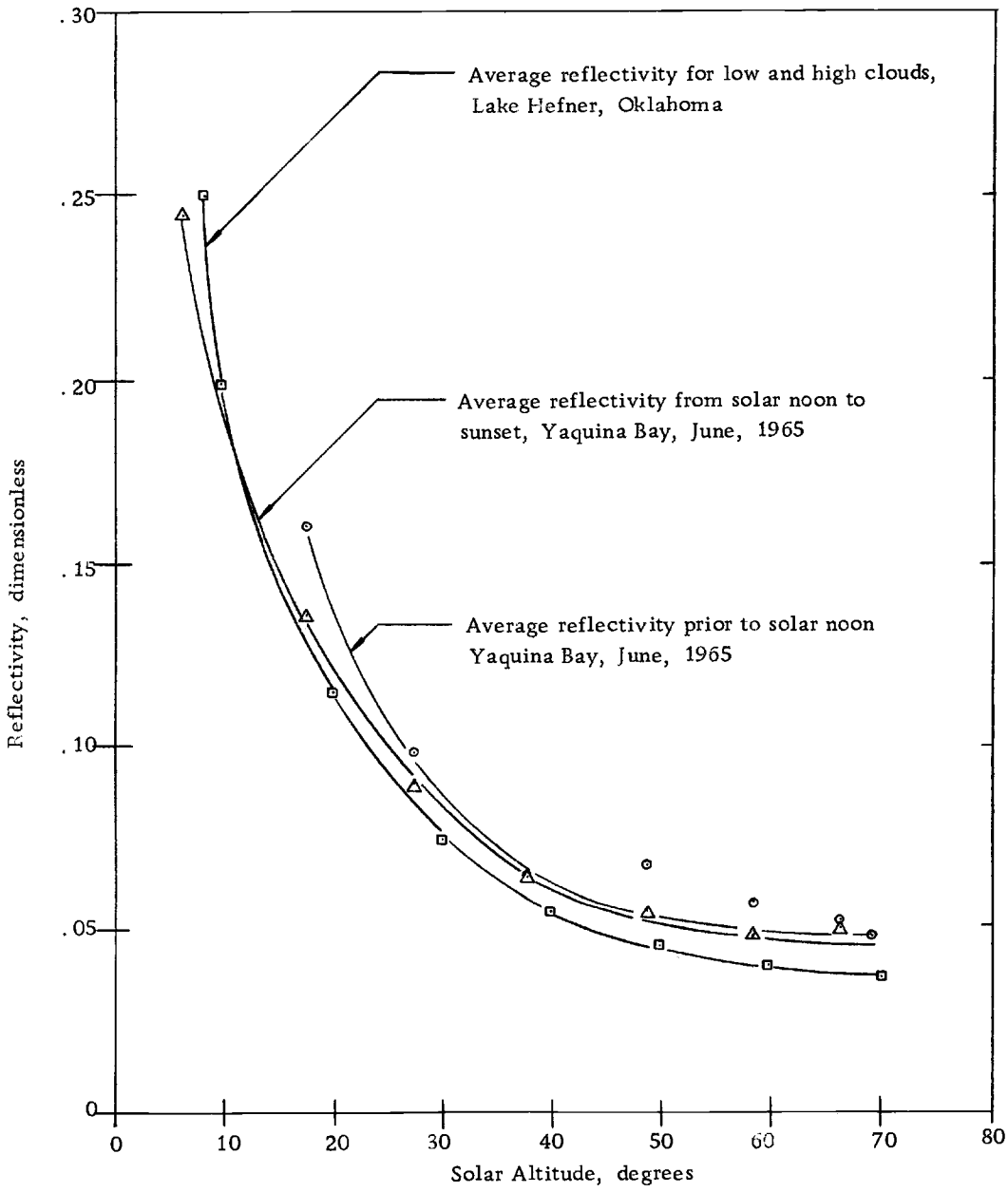


Figure 18. Effect of solar altitude on reflectivity.

At low solar altitudes, there is a broad range of reflectivities. Recalling that the actual value of solar radiation is small at low solar altitudes, one can see that the absolute error introduced by using an average value of reflectivity for all solar altitudes is very small. This is what is usually done in actual practice. Only seasonal changes in reflectivity are accounted for in most heat budget studies.

## Net Global Radiation

Net global radiation is useful for determining the amount of radiant energy absorbed by the sea surface. Net radiation *per se* does not generally appear in heat budget studies. The difference in upcoming and incoming global radiation is accounted for by the factor $Q_s(1-r)$, where $Q_s$ is the incoming global radiation, and r is the reflectivity.

The net global radiation was determined for Yaquina Bay by subtracting the reflected global radiation from the direct global radiation (Figure 16). Both reflected and direct global radiation were measured with Eppley pyranometers. The average value of net global radiation was 631.2 ly/day. Using the adjusted value of reflected radiation, which accounts for the obstruction of the dock, results in an average value of 627.4 ly/day.

Taking the ratio of the upcoming to incoming global radiation results in an average reflectivity of 0.068. Using the adjusted

upcoming global radiation value increases the average reflectivity to 0. 073.

Numerous values of average reflectivity appear in the literature. Schmidt (1915, in E. R. Anderson, 1954) discussed the theoretical reflectivity of both solar and sky radiation and obtained a theoretical value of 0. 17 for the reflectivity of sky radiation. This value was later shown by Burt (1953) to be invalid. Powell and Clarks's (1936) measurements gave a value for sky radiation under an overcast sky of 0. 08. Neiberger (1948) determined that the average reflectivity was 0. 105 and that reflectivity varied primarily with solar altitude and, to a lesser extent, with cloud thickness. He also indicated that for completely diffuse radiation Schmidt's theoretical value of 0. 17 was valid.

E. R. Anderson (1954) found that the average reflectivity at Lake Hefner was 0. 06. Burt (1954) prepared a table of reflectivities related to solar altitude, cloud cover and wind speed. He obtained values of reflectivity nearly equal to E. R. Anderson's. Both Burt's and Anderson's investigations show that the solar angle is the governing factor in the determination of reflectivity. Cox and Munk (1955) found that the reflectivity for a roughened sea varied between 0. 02 and 0. 15 for direct radiation and between 0. 04 and 0. 10 for sky radiation.

As indicated by these investigations, there is a general lack of

agreement concerning average values of reflectivity. However, it is generally accepted that the controlling factor in reflectivity is the solar altitude; reflectivity is affected to a much lesser degree by cloud cover, cloud thickness, and wind speed.

## Incoming Total Hemispherical Radiation

Average values of incoming total hemispherical radiation are useful in determining the amount of total energy incident on the sea surface. In turn, a knowledge of the absolute amount of total incoming radiant energy makes possible studies of its distribution and effects on life within the ocean, and its inclusion in air-sea exchange and heat budget studies. To date, no values of total hemispherical radiation measured over the ocean have appeared in the literature.

Incoming total hemispherical radiation was measured at selected times throughout the period of investigation with the new total hemispherical radiometer. The radiation data followed a regular and predictable pattern (Figure 19). Nocturnal values fluctuated over a range of only 0.026 ly/min. The small fluctuations were primarily due to changes in moisture content of the local air mass, i.e. changes in cloud amount, thickness, and height. However, the data do reflect the consistent nocturnal cloud conditions observed. Low level clouds, haze, or fog were noted in over 90%

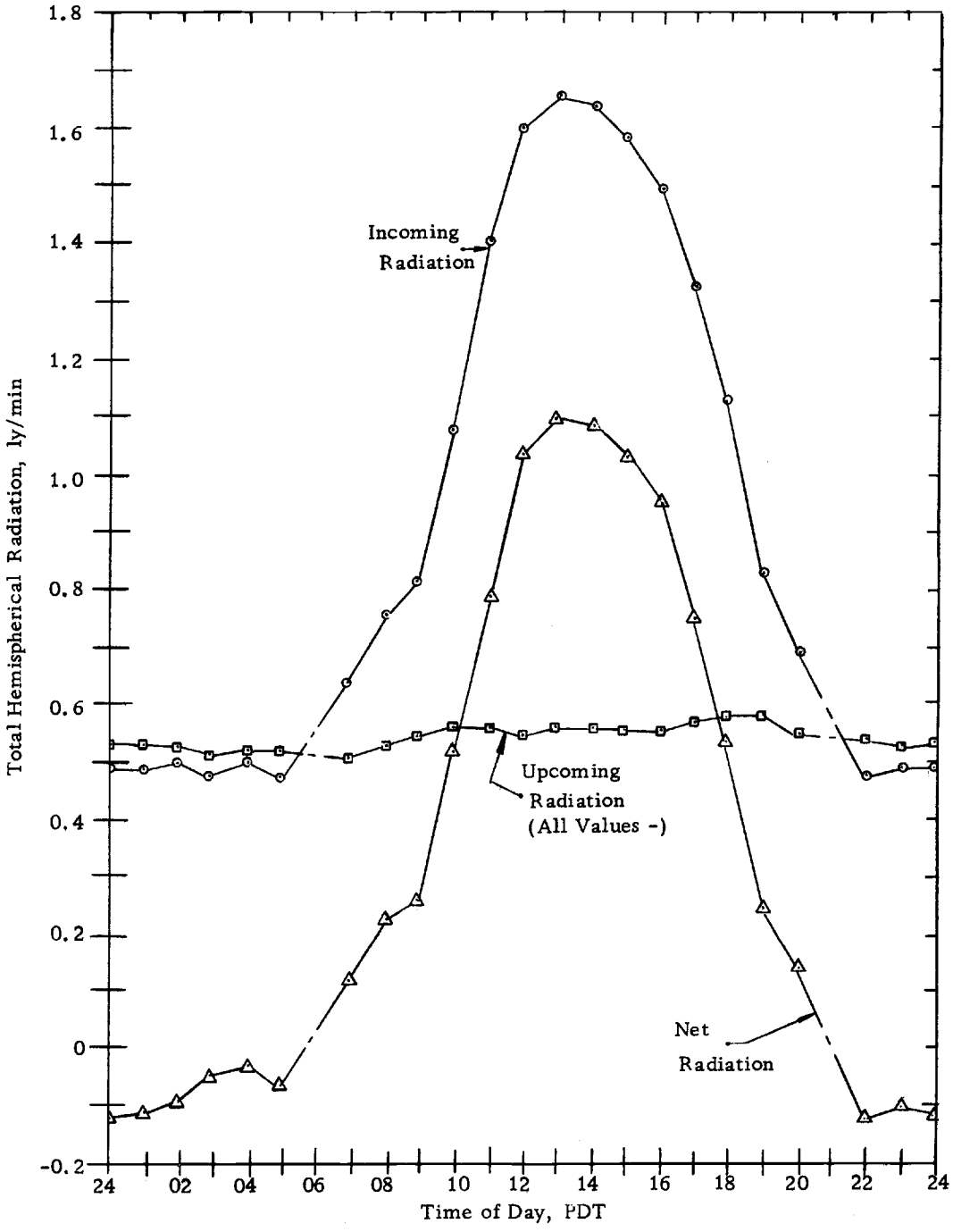


Figure 19. Average total hemispherical and net radiation measured at Yaquina Bay, June, 1965.

of the nocturnal weather observations. The average value of nocturnal incoming total hemispherical radiation was 0.491 ly/min.

Daytime observations of incoming total hemispherical radiation followed closely the shape of the incoming global radiation curve. Beginning at sunrise, the radiation continually increased to an average maximum of 1.660 ly/min, then continually decreased until sunset.

The average daytime value of incoming total hemispherical radiation was 1.192 ly/min. The average value for June was 1238.5 ly/day.

Upcoming Total Hemispherical Radiation

Average values of upcoming total hemispherical radiation are useful in determining the total amount of energy lost from the sea surface. This information plays as important a part in the overall energy exchange as does incoming total hemispherical radiation.

Upcoming total hemispherical radiation was measured at selected times throughout the period of investigation with the new total hemispherical radiometer facing the water. The radiometer was mounted, as was the Eppley pyranometer, at the end of a 16-foot boom attached to the dock at the Marine Science Laboratory. The inverted total hemispherical radiometer was subject to the same obstructions as the inverted pyranometer. Hence, the

upcoming total hemispherical radiation measured from sunrise to about 1000 local time cannot be considered valid regional data, but is applicable only to the immediate area.

Almost identical values were recorded each hour during the night (Figure 19). The difference between the maximum and minimum values was only 0.017 ly/min. The average nocturnal value was -0.525 ly/min.

If no obstructions blocked the reflected sun's rays from reaching the radiometer, the amount of upcoming total hemispherical radiation would increase rapidly after sunrise. The effect of the obstructions can be seen in Figure 19. The very gradual increase after sunrise is due to the loss of reflected solar radiation reaching the radiometer. After 1000 PDT, when the sun's rays were past the obstructions, there was a slight decrease in upcoming total hemispherical radiation until a minimum daytime value was reached. The maximum value of upcoming total hemispherical radiation was recorded between 1800 and 1900 PDT. The average daytime value of upcoming total hemispherical radiation was -0.556 ly/min. The average daytime value of upcoming total hemispherical radiation was adjusted by replacing the hourly values measured from sunrise to 1000 PDT with the corresponding hourly values measured from 1700 to 1900 PDT. The average value of daytime upcoming total hemispherical radiation obtained in this manner was -0.566 ly/min.

Integration of the adjusted upcoming total hemispherical radiation curve resulted in an average value for June of -728.3 ly/day.

Net Radiation

The difference between incoming and upcoming total hemispherical radiation is net radiation. Nocturnal net radiation was measured directly with the pair of new total hemispherical radiometers, one facing up, the other facing down. During the day, however, one of the two available radiometer recording channels was used with the Eppley pyranometer. Thus no direct measurements of net radiation were made during the day.

The nocturnal values shown in Figure 19 were measured directly. As expected, small negative fluctuations occurred. The values, averaging -0.092 ly/min, show that more radiant energy is being emitted than is being received by the water. Subtracting the average upcoming radiation from the average incoming radiation results in values averaging approximately 0.04 ly/min less than those measusured directly. This difference is relatively small and comprises only 4% of the daily net radiant energy. The fluctuations are again due to variations in the average moisture content of the air and changes in the surface water temperature. The combined effects are still small and are in agreement with the consistent nocturnal cloud conditions (discussed in the section on Incoming

Total Hemispherical Radiation) and small nocturnal surface water temperature changes.

The average daytime net radiation, shown in Figure 19, was obtained by subtracting the adjusted average upcoming total hemispherical radiation from the average incoming total hemispherical radiation. Immediately after sunrise, the net radiation rises to an average daily maximum of 1.101 ly/min at about 1300 PDT, then falls again to the negative nocturnal values.

The average daytime value of net radiation, computed from the adjusted values, was 0.626 ly/min. The average value for June was 510.2 ly/day.

Very few oceanic measurements of net radiation have been made. Ashburn (1963) published observations of net radiation taken during 1960 and 1961 at Ocean Weather Station PAPA. For these data, the average for June is 287 ly/day. It is interesting to note that for more than 70% of the days in June at Ocean Weather Station PAPA the sky was 7/8 covered with clouds. This is very nearly the average cloudiness observed during June, 1965, at Yaquina Bay.

## Incoming Long-wave Radiation

Nocturnal incoming long-wave radiation (Figure 20) was measured directly with the new total hemispherical radiometer. Small fluctuations occurred throughout the night. These expected

fluctuations were caused by the changes in the moisture content of the air, i. e. changes in cloud amount, height, and thickness. The magnitude of the nocturnal fluctuation, 0. 026 ly/min, was indicative of the fairly consistent nocturnal cloud coverage found over Yaquina Bay. During the five weeks of observations, the average value of nocturnal incoming long-wave radiation was 0. 491 ly/min.

Daytime incoming long-wave radiation was measured indirectly by subtracting the global radiation measured with the Eppley pyranometer from the total hemispherical radiation measured with the new total hemispherical radiometer (Figure 20). Shortly before sunrise, the average incoming long-wave radiation began to fall to the primary daytime minimum of 0. 409 ly/min. Radiation increased suddenly after 0800 PDT and leveled off at the midmorning maximum of 0. 474 ly/min. This increase can be explained by the decrease in cloudiness that occurred at this time of the morning. A decrease in cloudiness was observed every day when incoming long-wave radiation was being recorded. As the cloud cover decreased, the air temperature and vapor pressure increased rapidly, resulting in greater incoming long-wave radiation. The average value of daytime incoming long-wave radiation was 0. 446 ly/min. The average value for June was 610. 9 ly/day.

A difference of 0. 045 ly/min (about 9%) between the average nocturnal and daytime values was observed. There is no apparent

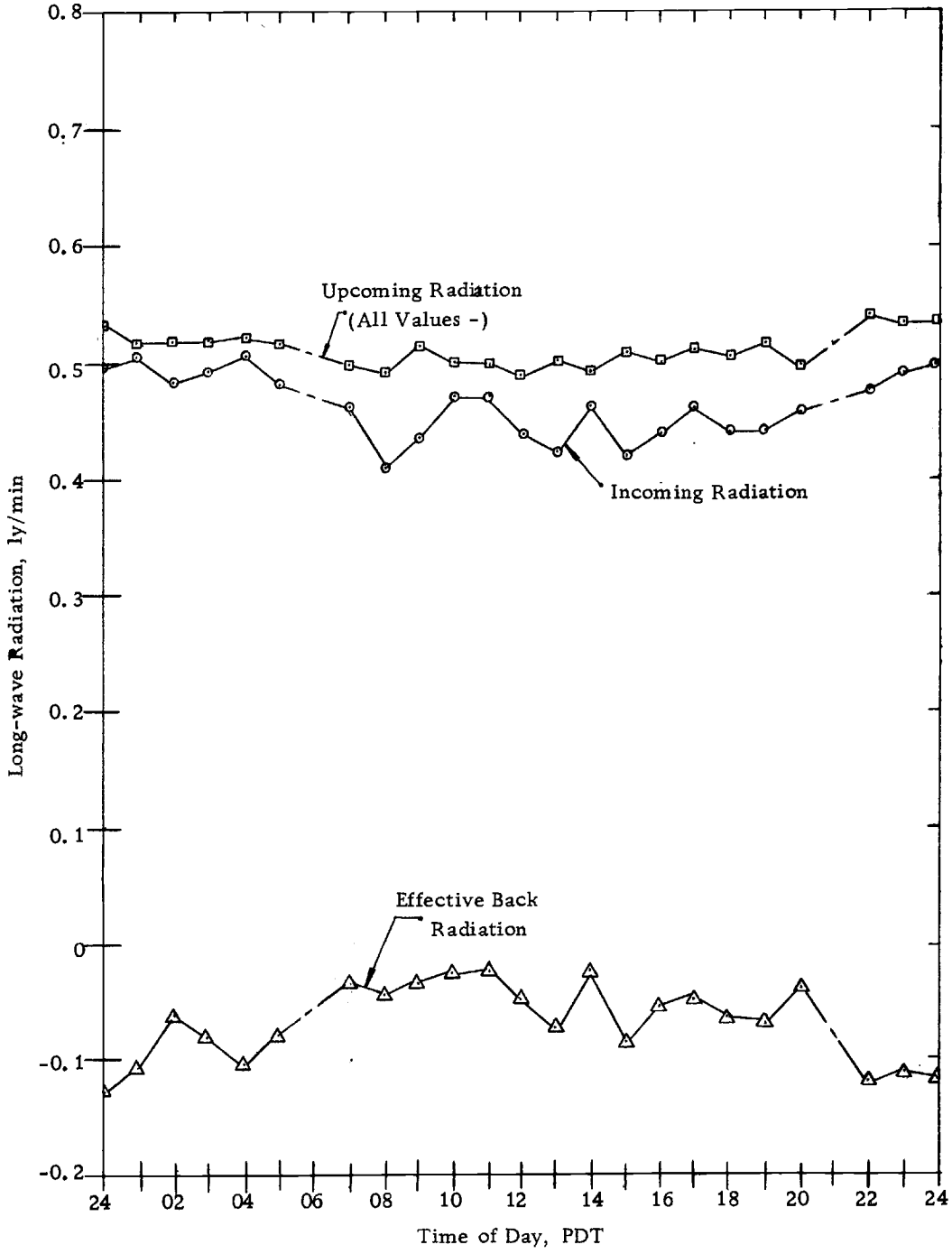


Figure 20. Average long-wave and effective back radiation measured at Yaquina Bay, June, 1965.

reason for this diurnal variation. During the day, when the lower atmosphere warms up, the vapor pressure increases. Water vapor in the atmosphere is an excellent absorber of long-wave radiation, except for the transparent band between approximately 8.5 and 11.0μ. Therefore, it is unreasonable to expect long-wave radiation to be less during the day. E.R. Anderson (1954) confirms this "unexpected" diurnal variation in incoming long-wave radiation in his work at Lake Hefner. He observed a decrease of approximately 50% between night and solar noon. Anderson states that such a decrease in long-wave radiation, if true, implies that some other component in the atmosphere radiates very strongly at the same wave lengths as the transparent band in the water vapor spectrum and, furthermore, has a large diurnal fluctuation. This is highly improbable and, Anderson concludes, the diurnal variation must be due to instrument error such as dependence of the flat-plate reflectivity on the sun's altitude.

The flat-plate transducer of the new radiometer has excellent cosine response when irradiated from a point source. However, in actual use, the transducer is receiving direct as well as diffuse radiation. During periods when the transducer is being irradiated by solar as well as long-wave radiation, the output emf of the instrument may be lower than the calibration constant indicates due to a change in the cosine response. A 9% decrease in the output is not

unreasonable in this situation. However, for energy budget studies, the daytime values should be increased by 9%. The adjusted average value of incoming long-wave radiation for June is then 665.9 ly/day.

Incoming long-wave radiation is dependent on many variables such as moisture, temperature, carbon dioxide and ozone. E. R. Anderson (1954) has shown that the amount of long-wave radiation can be determined conveniently from the local vapor pressure, cloud amount and height, and air temperature. Anderson defined an atmospheric radiation parameter, $\beta$, as the actual incoming long-wave radiation divided by the theoretical black-body energy radiating at the temperature of the air. He plotted $\beta$ against the local vapor pressure for a given cloud amount and height. Burt (1958) later published a set of composite curves based on Anderson's data.

It was anticipated that our observations of incoming long-wave radiation taken concurrently with observations of cloud amount, type, and height, and vapor pressure measured at the instrument level, could be checked against Anderson's data. Observations of radiation were made under sky conditions varying from clear to 10 tenths coverage, but unfortunately, the local vapor pressure varied over only about 25% of the vapor pressure range measured by Anderson. Also, 91% of the clouds observed were low clouds (height less than 6,500 feet). Only 2% of the clouds were classed as middle clouds (height between 6,500 and 20,000 feet), and 7% of the clouds were

classed as high clouds (height greater than 20,000 feet). No attempt was made, therefore, to plot a complete set of curves similar to Anderson's.

However, sufficient data on the atmospheric radiation parameter as a function of local vapor pressure are available for clear skies and low clouds of scattered (0.1 to 0.5 coverage), broken (0.6 to 0.9 coverage), and overcast conditions. These data are shown in Figure 21. The vapor pressure ranged generally between 0.30 and 0.36 inches (Hg), an insufficient range for computing curves comparable to Anderson's. The narrow range of vapor pressures indicates that during the period of measurements no major change in air mass occurred. For comparison, E.R. Anderson's (1954) curves are also plotted in Figure 21. The data suggest that fairly close agreement between Anderson's data and data taken in an oceanic environment is possible.

Several general statements can be made from an examination of Figure 21. The radiation is the least for clear skies and appears to increase with both cloud amount and vapor pressure. The incoming long-wave radiation approaches the theoretical black-body radiation under overcast skies, particularly under higher vapor pressures.

## Upcoming Long-wave Radiation

Upcoming long-wave radiation data were taken in a manner

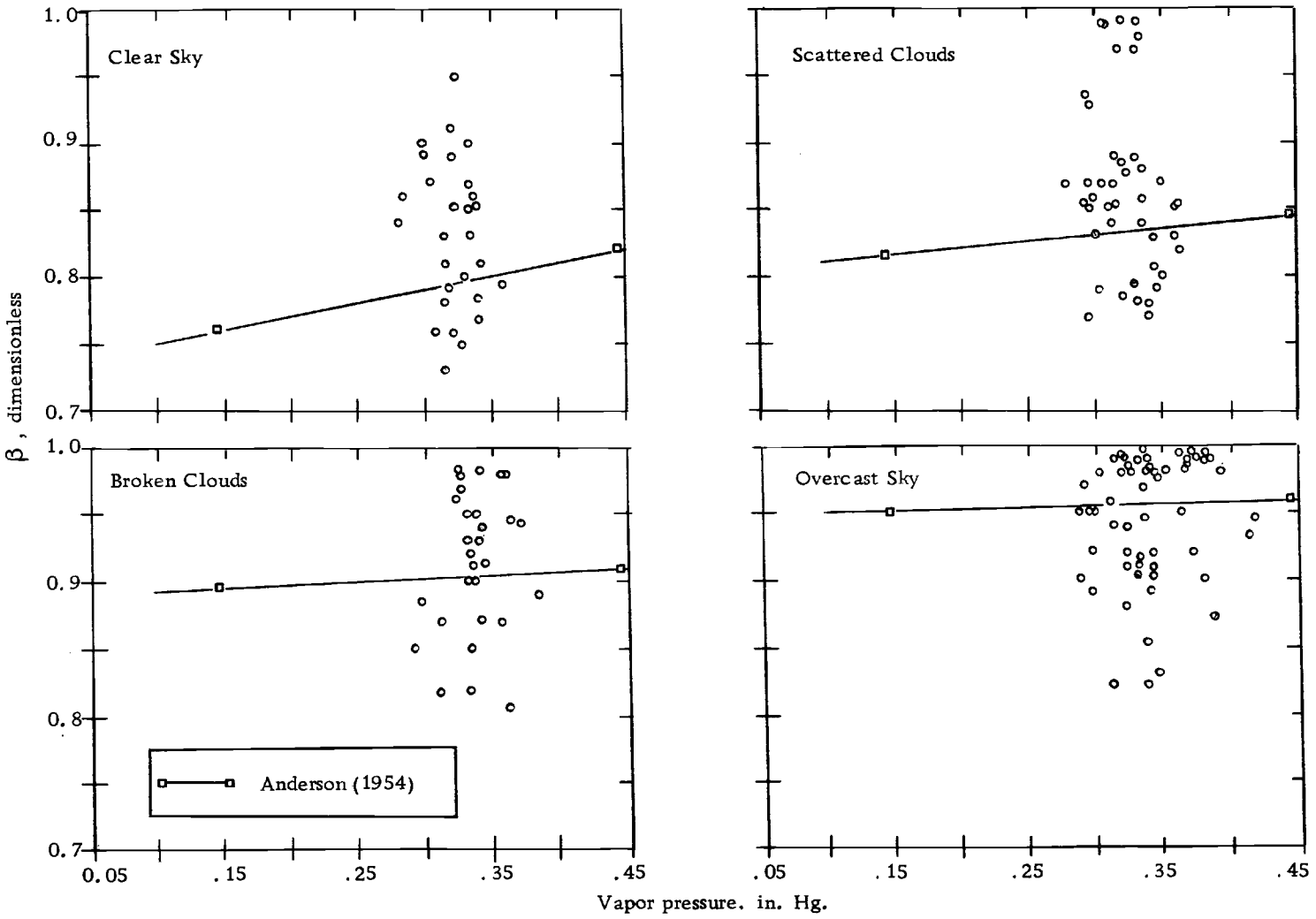


Figure 21. Atmospheric radiation parameter, $\beta$, as a function of local vapor pressure for clear skies and low clouds, Yaquina Bay, June, 1965.

similar to those of incoming long-wave radiation; i. e. nocturnal radiation was measured directly and daytime radiation was measured indirectly. The average nocturnal upcoming long-wave radiation (Figure 20) increased continually from sunset until shortly before midnight local time when a maximum value of -0. 537 ly/min was reached. The average nocturnal value of upcoming long-wave radiation was -0. 525 ly/min.

A slight increase in upcoming long-wave radiation was observed just after sunrise. Small fluctuations varying between -0. 490 and -0. 516 ly/min continued throughout the day. The average daytime value of upcoming long-wave radiation was -0. 512 ly/min. The average value for June was -673. 1 ly/day.

Long-wave radiation from a body of water, F, is usually computed from the modified Stefan-Boltzmann equation, $F = e\sigma T_s^4$, where e is the surface water emissivity, $\sigma$ is the universal Stefan-Boltzmann constant, and $T_s$ is the absolute surface water temperature. For a perfect black-body surface, e = 1. 0; for all other surfaces $e < 1$.

Because surface emissivity is defined for a specific wave length only, a new term, e', was introduced for this investigation. The term, e', is defined as the ratio of the measured upcoming long-wave radiation (including the reflected long-wave radiation) to the energy emitted by the water surface, assuming the surface

radiates as a perfect black body. Then, the Stefan-Boltzmann equation may be written as:

$$R_s = e' \sigma T_s^4 \tag{18}$$

where $R_s$ is the total upcoming long-wave radiation from the water surface.

Various values of $e'$ for a saline water surface have been proposed. For example, Sverdrup (1943, in Lane (1965)) used a value of 0.94 in his back radiation calculations; E.R. Anderson (1954) used a value of 0.97 in his work at Lake Hefner. Sverdrup does not account for reflected long-wave radiation in his value of $e'$.

Values of $e'$ were computed for all available upcoming long-wave radiation data. Nocturnal values of $e'$ averaged 0.98 while daytime values averaged 0.94. Therefore, the average value most representative of the area under investigation is 0.96. It is proposed, then, that using the equation

$$R_s = 0.96 \sigma T_s^4 \tag{19}$$

would produce values of upcoming long-wave radiation values close to the actual conditions found in the oceanic environment.

## Effective Back Radiation

Effective back radiation is defined as the difference between upcoming and incoming long-wave radiation. During the day, four

integration channels would be required to make this measurement. Since only two integration channels were available at any one time, effective back radiation could be measured directly only at night. Because global radiation is not received at night, nocturnal values of effective back radiation are identical to nocturnal values of net radiation. Therefore, the discussion of nocturnal net radiation (pages 94 through 95) also applies to nocturnal effective back radiation. Daytime values of incoming and upcoming long-wave radiation (Figure 20), recorded during adjacent weeks, were considered as concurrent measurements which are usable for determining daytime values of effective back radiation.

At night, upcoming long-wave radiation was greater than incoming long-wave radiation. The average nocturnal effective back radiation was -0.092 ly/min. The consistent difference between incoming and upcoming long-wave radiation is immediately obvious when one examines the two sets of data separately.

The daytime values of effective back radiation fluctuated over a range of 0.053 ly/min. The greatest fluctuation was recorded for three to four hours after sunrise and was caused by the sudden change in incoming long-wave radiation during that period. A detailed discussion of the early morning change in incoming long-wave radiation appears in the section on Incoming Long-wave Radiation. The average value of daytime effective back radiation was -0.055

ly/min. The average value for June was -70.6 ly/day. Using the adjusted daytime value of incoming long-wave radiation resulted in an average value of -66.4 ly/day.

Effective back radiation, $Q_b$, is of prime importance in heat budget studies. Tabata (1961), using constants and charts prepared by E.R. Anderson (1954) derived the following empirical equation for his heat budget analysis at Ocean Weather Station PAPA, in the North Pacific Ocean:

$$Q_b = 1.141\left\{\theta_s^4 - \theta_a^4\left[(0.74 + 0.025ce^{-0.0584h}) + (0.0049 - 0.00054ce^{-0.06h})e_a\right]\right\} 10^{-7} \qquad (20)$$

where $\theta_s$ = temperature of the sea surface, °K

$\theta_a$ = temperature of the air, °K

c = cloud coverage, tenths

e = base of natural logarithms

h = cloud height, thousands of feet

$e_a$ = vapor pressure of the atmosphere where the air temperature is measured, in millibars.

Tabata computed the effective back radiation at PAPA for the month of June during 1957-58. The average for both years was approximately -80 ly/day.

Equation (20) was also used by Lane (1965) in his heat budget analysis of the area off the coast of Oregon. Using marine weather

data for June from ten successive years, he computed an average effective back radiation of -68 ly/day.

Roden (1959) and Wyrtki (1965), using a semi-empirical equation derived by Beriland (1952, in Roden (1959)), have computed the effective back radiation for the Eastern North Pacific Ocean. Beriland's equation is given as:

$$Q_b = -s\sigma\theta_s^4(0.39-0.057\sqrt{e_a})(1-k''c^2)+4s\theta_s^3(\theta_s-\theta_a) \qquad (21)$$

where $s$ = ratio of the radiation of the sea surface to a black body, dimensionless

$k''$ = constant in table prepared by Budyko, dimensionless.

The other terms were defined previously. Roden classified the California current region into eight areas of which area "A" is closest to the area immediately off the Oregon coast; its northern boundary is within four degrees latitude of Newport, Oregon. Using climatological data obtained from various sources, Roden found the effective back radiation for June in area "A" to be -114 ly/day.

Wyrtki (1965) computed average effective back radiation for the North Pacific Ocean for individual months based on marine weather reports from 14 years (1947-1960). His average annual effective back radiation for the area immediately off the coast of Oregon is given as -110 ly/day. Lane's (1965) annual value agrees very closely with this number.

Two other empirical equations for computing effective back radiation over the oceans merit mentioning. Brunt's empirical formula is given by Sverdrup (1943) as:

$$Q_b = -\sigma \theta_s^4 (0.56 - 0.08\sqrt{e_a})(1-0.83c) \quad (22)$$

Recently, Möller (in Dietrich, 1963) suggested using the cloud correction factor (1-0.765c). The effective back radiation also depends upon the altitude and density of the clouds. With a sky completely covered with cirrus, Möller's cloud cover correction factor is 0.75; with altostratus, 0.4; and with stratocumulus, 0.1 (Laevastu, 1960). Raphael (1962) suggests computing effective back radiation by the following equation:

$$Q_b = 0.97\sigma(\theta_s^4 - \beta\theta_a^4) \quad (23)$$

where values of $\beta$ are given by Raphael from Anderson's (1954) data modified by Burt (1958).

Sverdrup, Johnson, and Fleming (1942) and Laevastu (1960) published curves of effective back radiation to a clear sky as a function of sea surface temperature and relative humidity. These curves must be corrected for cloud coverage to yield meaningful values.

Table 7 summarizes computed effective back radiation from sources mentioned above and effective back radiation measured at

Yaquina Bay during June, 1965. Averages of the meteorological and oceanographic parameters observed at Newport were used in the computations.

Table 7. Comparison of effective back radiation determined from empirical formulae or graphs by the authors listed and effective back radiation value of -71 ly/day measured at Yaquina Bay, June, 1965.

| Equation | Reference | Computed ly/day | Difference ly/day | Difference % |
|---|---|---|---|---|
| (20) | Tabata (1961) | - 9 | -62 | 87 |
| (21) | Roden (1959) | -108 | 37 | 52 |
| (22) | Sverdrup (1945) | - 85 | 14 | 20 |
| (23) | Raphael (1962) | - 98 | 27 | 39 |
| | Sverdrup, Johnson and Fleming (1942), p. 111. | -108[1] | 37 | 52 |
| | Laevastu (1960) p. 44 | - 78[1] | 7 | 10 |

[1] Values are corrected by applying Möller's cloud correction factor of 0.426

These data indicate that the present empirical equations relating effective back radiation to the various meteorological and oceanographic parameters are not usable with short-term data if accuracies better than 10% are required. Laevastu's method of determining effective back radiation appears most promising of the

several methods tested. It is of interest to note that Lane's (1965) climatological value of effective back radiation of -68 ly/day, computed using Tabata's equation, is within 5% of the measured value. This is indicative of the use for which the above equations were intended; that is, the accuracy is increased by using climatological rather than short-term data.

# SUMMARY OF FINDINGS AND SUGGESTIONS FOR FUTURE RESEARCH

## Summary

The results of the measurement of solar and long-wave radiation in an oceanic environment are reported in this investigation. The Eppley pyranometer was used to measure solar radiation. Unfortunately, no acceptable pyrgeometers were available to measure long-wave radiation. A program was then undertaken to design, construct, and test a radiometer that would measure total hemispherical radiation in an oceanic environment with a suitable degree of accuracy. A specially designed, wind oriented, total hemispherical radiometer that has the following characteristics was constructed: 1) The radiometer gives an output signal that is independent of the energy fluctuations in non-radiant energy sources. The capability of the radiometer to be directed downwind by the natural wind has essentially eliminated the undesirable convective energy produced by crosswinds. 2) The response of the radiometer is almost totally independent of the wave length of the incident radiation. 3) The time constant of the radiometer is approximately nine seconds. 4) The radiometer is constructed to withstand the corrosive nature of the marine environment. 5) The instrument is lightweight and compact, and thus is ideal for mounting on a boom to measure

upcoming radiant energy from a body of water.

The new radiometer required a special data-logging system which was also designed, constructed, and tested. Provisions were made in the electronic readout for integration and display of the incoming signal. Integrated values of radiation were automatically recorded each hour and the data stored on paper tape for later analysis.

Data were recorded continuously for five weeks during June and July, 1965, from the docking facility at the Marine Science Laboratory near Newport, Oregon. Meteorological and oceanographic data taken at the dock during the investigation show values almost identical with those recently reported by Lane (1965) for the area immediately off the Oregon coast. The radiant energy flux measured from the dock was then considered as very nearly representative of the flux of radiant energy in an oceanic environment.

Nine sources and wave lengths of radiation were measured at selected times during the investigation. The primary conclusions regarding each are discussed below.

Direct global radiation: The average incoming global radiation was 676.9 ly/day; the average daily maximum was 1.238 ly/min. The effects of clouds on incoming radiation exhibit a curvilinear relationship when plotted against solar altitude. Increasing cloud cover decreases the radiation measured at all solar altitudes. The

incoming global radiation was computed from empirical formulae used in various heat budget analyses. Lumb's (1964), Ashburn's (1963), and Laevastu's (1960) formulae appear most promising for predicting values within 10% of the measured ones.

Reflected global radiation: The average reflected global radiation was -49.5 ly/day. The early morning values were adjusted to account for the obstruction presented to the inverted pyranometer by the dock. The reflected energy is consistent with that computed by multiplying generally accepted values of reflectivity by incoming global radiation. E. R. Anderson's (1954) curves of reflectivity versus solar altitude were compared to curves plotted from the data taken at Yaquina Bay and were found to be in very close agreement.

Net global radiation: The average net global radiation was 627.4 ly/day. The average reflectivity (0.073) was computed by taking the ratio of upcoming global radiation to incoming global radiation. This value agrees in the same order of magnitude with generally accepted values of average reflectivity.

Incoming total hemispherical radiation: The average incoming total hemispherical radiation was 1238.5 ly/day. Amounts varied between 1.660 and 0.478 ly/min. Small nocturnal fluctuations, due primarily to changes in moisture content of the local air mass, were observed. The small fluctuations are indicative of the consistent cloud coverage that was observed during the night at Yaquina

Bay. Daytime observations of incoming total hemispherical radiation, as expected, followed closely the shape of the incoming global radiation curve.

Upcoming total hemispherical radiation: The average upcoming total hemispherical radiation was -728.3 ly/day. Actual amounts varied between 0.585 and 0.516 ly/min. Almost identical values were observed every hour during the night. The maximum value of upcoming total hemispherical radiation was recorded in the late afternoon.

Net radiation: The average net radiation was 510.2 ly/day. The average nocturnal value was -0.092 ly/min, and the average daytime value was 0.626 ly/min. As expected, there was a net loss of radiant energy from the water to the sky during the night. This trend was reversed during the day. Lane's (1965) climatological value of net radiation for the area immediately off the Oregon coast was about 11% higher than the value measured at Yaquina Bay during June, 1965.

Incoming long-wave radiation: The average incoming long-wave radiation was 665.9 ly/day. A 9% difference between the average nocturnal and daytime values was observed. This unexpected decrease can be explained by a change in the cosine response of the radiometer when irradiated by both direct and diffuse radiation. To account for this apparent diurnal variation, the average value

given above has been increased by 9% over the average amount actually measured. The radiation parameter, $\beta$, defined by E. R. Anderson (1954), was plotted for clear skies and low clouds of scattered, broken, and overcast conditions. Over the narrow range of vapor pressures observed at Yaquina Bay, average values of $\beta$ agreed with values of $\beta$ observed at Lake Hefner, Oklahoma. From these plots, it was evident that incoming long-wave radiation was the least for clear skies and increased with both cloud amount and vapor pressure. The incoming long-wave radiation approached the theoretical black-body radiation under overcast skies, particularly under the higher vapor pressures.

Upcoming long-wave radiation: The average upcoming long-wave radiation was -673.1 ly/day. A new term, e', was defined as the ratio of the measured upcoming long-wave radiation (including the reflected long-wave radiation) to the energy emitted by the water surface, assuming it radiates as a perfect black body. This term was then introduced into the Stefan-Boltzmann equation. Values of e' were computed for all available upcoming long-wave radiation data. The average daily value of e' was 0.96.

Effective back radiation: The average effective back radiation was -66.4 ly/day. As expected, greater negative back radiation was observed during the night than during the day. The effective back radiation was computed from several empirical formulae used

in various heat budget analyses. All of the computed values differed from the measured value by 10% or more. It is concluded that these formulae do not describe short-term conditions but are useful only for describing average conditions over a long period of time.

## Suggestions for Future Research

1. It is evident that additional continual measurements extending over several years are necessary to fully understand the seasonal trends of radiant energy exchange. Therefore, definite steps should be taken to insure the permanent placement and proper maintenance of the instruments, so that quality data can be secured.

2. Throughout this investigation further modifications on the new radiometer were made in an attempt to improve the instrument. One such modification came from a suggestion of L. J. Anderson (1954): "Accurate terrestrial [long-wave] radiation values might be obtained by using a glass-covered flat plate for obtaining solar-energy values. If the covered and uncovered flat plates were connected in series with opposite polarity, the resulting recorded value should approximate the terrestrial energy flux."

High quality plate glass was placed over the transducer of the total hemispherical radiometer, and its output under a given irradiation was compared to the output of the Eppley pyranometer under similar irradiation. Depending on the lamp voltage setting, and

how long the lamp was allowed to irradiate the transducer, readings were from 10 to 50% greater than those from the Eppley pyranometer. The initial readings were expected to be lower due to the lack of 100% transmission of incident short-wave radiation. However, the greater signal could be caused by the glass reflecting some of the transducer-emitted long-wave radiation back to the transducer which would "see" the energy as part of this incident radiation.

Additional tests are needed before the higher readings can be fully explained. With the proper adjustments, either to the plate glass mounting or to the calibration constant, the new radiometer can be adapted to measure solar as well as total hemispherical radiation.

# BIBLIOGRAPHY

Aagard, Roger L. 1958. Convection free instrument for measuring infrared radiation in the atmosphere. Review of Scientific Instruments 29(11):1011-1015.

Abbot, C. G. 1913. Measurements of solar radiation. Astrophysical Journal 37:130-144.

Anderson, Ernest R. 1954. Energy-budget studies. In: Water loss investigations: Lake Hefner studies, Technical Report. Washington. p. 71-119. (U. S. Geological Survey. Professional paper 269)

Anderson, Lloyd J. 1954. Instrumentation for mass-transfer and energy-budget studies. In: Water loss investigations: Lake Hefner studies, Technical Report. Washington. p. 35-45. (U. S. Geological Survey. Professional paper 269)

Ångström, Anders. 1919. A new instrument for measuring sky radiation. Monthly Weather Review 47:795-797.

Ashburn, Edward V. 1963. The radiative heat budget at the ocean-atmosphere interface. Deep Sea Research 10:597-606.

Black, J. N. 1960. The distribution of solar radiation over the earth's surface. Archiv of Meteorologie, Geophysik und Bioklimatologie, Ser. B 10:182-192.

Boelter, L. M. K., H. F. Poppendiek and J. T. Gier. 1944. An investigation of aircraft heaters XVII-experimental inquiry into steady state unidirectional heatmeter corrections. Washington, National Advisory Committee for Aeronautics. 25 p. (Advanced Restricted Report, No. 4H09)

Boudreau, R. D. 1964. Skin temperature of the sea as determined by radiometer. Master's thesis. College Station, Texas A&M University. 68 numb. leaves.

Burt, Wayne V. 1953. A note on the reflection of diffused radiation by the sea surface. Transactions of the American Geophysical Union 34:199-200.

Burt, Wayne V. 1954. Albedo over wind-roughened water. Journal of Meteorology 11(4):283-290.

Burt, Wayne V. 1958. Heat budget terms for Middle Snake River reservoirs. Corvallis. 23 p. (Oregon State University. Technical Report 6)

Burt, Wayne V. and W. Bruce McAllister. 1959. Recent studies in the hydrography of Oregon estuaries. In: Collected Reprints. Vol. I. Oregon State University Dept. of Oceanography p. 40-52.

Bushnell, R. H. and V. E. Suomi. 1961. Experimental flight verification of the economical net radiometer. Journal of Geophysical Research 66(9):2843-2848.

Cox, C. and W. Munk. 1955. Some problems in optical oceanography. Journal of Marine Research 14:63-78.

Dietrich, Günter. 1963. General oceanography. New York, Interscience Publishers. 588 p.

Drummond, A. J., Chief Research Physicist for Eppley Laboratory, Inc. Nov. 27, 1964. Personal communication. Newport, R. I.

Dunkle, R. V. et al. 1949. Non-selective radiometers for hemispherical irradiation and net radiation interchange measurements. Berkeley. 27 numb. leaves. (University of California. Dept. of Engineering. Thermal radiation Report No. 9, Contract NR-onr - 295 Task I NR -015-202)

Elder, Robert B. 1960. Radiation measurements. In: Oceanographic Instrumentation: Final Report of the Committee on Instrumentation. Washington. Various paging. (U. S. Navy Hydrography Office. SP-41)

Eppley Laboratory, Inc. 1960. Parsons' Optical Black Lacquer. Newport, R. I. 3 p. (Processed)

Eppley Laboratory, Inc. 1964. The Eppley pyranometer. Newport, R. I. 4 p. (Bulletin no. 2)(Processed)

Falkenberg, G. 1947. Ein Vibrationspyranometer. Zeitschrift fur Meteorologie 1(11-12):372-374.

Fritschen, L. J. 1960. Construction and calibration details of the thermal-transducer-type net radiometer. Bulletin of the American Meteorological Society 41(4):180-183.

Fritschen, L. J. and W. R. van Wijk. 1959. Use of an economical thermal transducer as a net radiometer. Bulletin of the American Meteorological Society 40(6):291-294.

Funk, J. P. 1959. Improved polythene-shielded net radiometer. Journal of Scientific Instruments 36:267-270.

Fuquay, Don and K. Buettner. 1957. Laboratory investigation of some characteristics of the Eppley pyrheliometer. Transactions of the American Geophysical Union 38(1):38-43.

Gates, David M. 1962. Energy exchange in the biosphere. New York, Harper and Row. 151 p.

Gier, J. T. and L. M. K. Boelter. 1941. The silver-constantan plated thermopile. In: Temperature, its measurement and control in science and industry. New York, Reinhold Publ. Corp. p. 1284-1292.

Gier, J. T. and R. V. Dunkle. 1951. Total hemispherical radiometers. Proceedings of the American Institute of Electrical Engineers 70:339-343.

Goldwater, F. J. 1965. Integrator for net radiometer. Solar Energy 9(1):4-6.

Gorczynski, L. 1924. On a simple method of recording the total and partial intensities of solar radiation. Monthly Weather Review 52:299.

Haltner, G. J. and F. L. Martin. 1957. Dynamical and physical meteorology. New York, McGraw-Hill. 470 p.

Hardy, J. D. 1934. The radiation of heat from the human body. Journal of Clinical Investigations 13:593-604.

Hexcel Products Inc. 1959. Preliminary findings on air directionalizing characteristics of Hexcel aluminum honeycomb. Berkeley, Cal. 7 p. (Technical Services Bulletin TR-21) (Processed)

Houghton, J. T. and A. W. Brewer. 1954. A new radiometer. Journal of Scientific Instruments 31(5):184-187.

International Geophysical Year, (IGY). 1958. Instruction Manual, Part VI: Radiation instruments and measurements. London, Pergamon Press. 466 p.

Jerger, Joseph Jr. Infrared and Electro-Optics Div. of Servo Corp. of America. Dec. 18, 1964. Personal communication. Hicksville, New York.

Johnson, D. S. 1956. Progress report on radiometer tests December 1956. Washington, U. S. Weather Bureau. 20 p.

Karoli, A. R., A. K. Ångström and A. J. Drummon. 1960. Dependence on atmospheric pressure of the response characteristics of thermopile radiant energy detectors. Journal of the Optical Society of America 50(8):758-763.

Kimball, H. H. 1928. Amount of solar radiation that reaches the surface of the earth on the land and on the sea, and methods by which it is measured. Monthly Weather Review 58:43-52.

Kimball, H. H. and H. E. Hobbs. 1923. A new form of thermoelectric recording pyrheliometer. Monthly Weather Review 51:239-242.

Kondrat'yev, K. Ya. 1965. Radiative heat exchange in the atmosphere. Tr. by O. Tedder. Oxford, Pergamon Press. 411 p.

Kuhn, P. M. 1961. Accuracy of the airborne economical radiometer. Monthly Weather Review 89(8):285-287.

Kulm, LaVerne D. 1965. Sediments of Yaquina Bay, Oregon. Ph. D. thesis. Corvallis, Oregon State University. 184 numb. leaves.

Laevastu, T. 1960. Factors affecting the temperature of the surface layer of the sea. Societas Scientiarum Fennica, Commentationes Physico-Mathematicae 25(1):1-136.

Lane, Robert K. 1965. Climate and heat exchange in the oceanic region adjacent to Oregon. Ph. D. thesis. Corvallis, Oregon State University. 115 numb. leaves.

Latimer, J. R. 1962. Laboratory and field studies of the properties of radiation instruments. Dept. of Transport, Canada. 13 p. (Technical Report 414)

Latimer, J. R. and V. Marsh. 1962. Instrumentation for automatic integration of solar radiation measurements. Dept. of Transport, Canada. 7 p. (Technical Report 413)

Lowry, William P. 1957. An inexpensive field instrument for non-selective net radiation measurements. Ecology 38(1):152-155.

Lumb, F. E. 1964. The influence of cloud on hourly amounts of total solar radiation at the sea surface. Quarterly Journal of the Royal Meteorological Society 90(383):43-56.

Lussier, O. E. Jr., Sales Manager, Valpey Corp. Dec. 11, 1964. Personal communication. Hollister, Mass.

MacDowall, J. 1955. A total radiation fluxmeter. Meteorological Magazine 84(993):65-71.

Marvin, C. F. and H. H. Kimball. 1926. Solar radiation and weather forecasting. Journal of the Franklin Institute 202(3): 273-281.

Maughan, Paul M. and Roderick S. Mesecar. 1965. A solar and long-wave radiation measuring system for shipboard use. In: Transactions of the Joint Conference and Exhibit, Ocean Science and Ocean Engineering, Vol. 1. Washington, Marine Technology Society. p. 373-383.

McAlister, E. D. 1965. A two-wave length microwave radiometer for measurement of the total heat exchange at the air-sea interface. Applied Optics 4(1):145-146.

McGuire, J. H. and H. Wraight. 1960. Radiometer for field use. Journal of Scientific Instruments 37:128-130.

Minard, David R. 1965. Solar radiation measured at the sea surface off Oregon during summer 1963. Master's thesis. Corvallis, Oregon State University. 74 numb. leaves.

Moll, W. J. H. 1923. A thermopile for measuring radiation. Proceedings of the Physical Society of London 35:257-260.

Monteith, J. L. 1959. Solarimeter for field use. Journal of Scientific Instruments 36(8):341-346.

Mörikofer, W. 1939. Meteorologische Strahlunssmessmethoden. In: Handbuch der Biologischen Arbeitsmethoden. Berlin, Urban and Schwarzberg. p. 4005-4245.

Neiburger, M. 1948. The reflection of diffuse radiation by the sea surface. Transactions of the American Geophysical Union 29(5):647-652.

Peterson, D. H., Commercial Contract Sales, Bausch & Lomb Inc. Dec. 15, 1964. Personal communication. Rochester, New York.

Poppendick, Heinz, President of Geonetics Corp. Aug. 11, 1965. Personal communication. San Diego, Cal.

Portman, Donald J. 1957. Gier and Dunkle heat flow meters and heat storage variations - Johns Hopkins University. In: Exploring the atmosphere's first mile, ed. by Heinz H. Lettau and Ben Davidson. New York, Pergamon Press. p. 64-66.

Portman, Donald J., Professor of Meteorology, University of Michigan. June 29, 1964. Personal communication. Ann Arbor, Mich.

Powell, Wilson M. and George L. Clark. 1936. The reflection and absorption of daylight at the surface of the ocean. Journal of the Optical Society of America 26:111-120.

Pritchard, D. W. 1955. Estuarine circulation patterns. Proceedings of the American Society of Civil Engineers 81(717):1-11.

Raphael, Jerome M. 1962. Prediction of temperature in rivers and reservoirs. Journal of the Power Division, Proceedings of the American Society of Civil Engineers. 88(PO2):157-181.

Roden, G. I. 1959. On the heat and salt balance of the California current region. Journal of Marine Research 18(1):36-61.

Roll, H. U. 1965. Physics of the marine atmosphere. New York, Academic Press. 426 p.

Schoffer, P. and V. E. Suomi. 1961. A direct current motor integrator for radiation measurements. Solar Energy 5(1):29-32.

Skeib, Günter. 1953. Ein rotierender Strahlungsumsatzmesser mit induktiver Ubertragung der Messspannung. Zeitschrift für Meteorologie 7(6):167-171.

Suomi, V. E., Matti Franssila, and N. F. Islitzer. 1954. An improved net-radiation instrument. Journal of Meteorology 11:276-282.

Suomi, V. E. and P. M. Kuhn. 1958. An economical net radiometer. Tellus 10:160-163.

Stern, Sidney C. and Frederick Schwartzmann. 1954. An infrared detector for measurement of the back radiation from the sky. Journal of Meteorology 11(2):121-129.

Stoll, A. M. 1954. A wide-range thermistor radiometer for the measurement of skin temperature and environmental radiant temperature. Review of Scientific Instruments 25:184-187.

Sverdrup, H. U. 1943. Oceanography for meteorologists. New York, Prentice-Hall. 246 p.

Sverdrup, H. U., M. W. Johnson and R. H. Fleming. 1942. The oceans. Englewood Cliffs, N. J., Prentice-Hall. 1087 p.

Tabata, Susumu. 1961. Temporal changes of salinity, temperature, and dissolved oxygen content of the water at Station "P" in the Northeast Pacific Ocean, and some of their determining factors. Journal of the Fisheries Research Board of Canada 18(6):1073-1124.

Tunmore, B. G. 1962. A simple radiometer for the measurement of radiative heat exchange between buildings and the environment. Journal of Scientific Instruments 39(5):219-221.

U. S. Dept. of Commerce. 1962. Manual of radiation observations. Washington. 87 p.

U. S. Naval Observatory. 1963. American ephemeris and nautical almanac. Washington. 518 p.

Whittier, A. 1964. Integrating instrument for measuring solar radiation. Solar Energy 8(4):134-136.

Wilson, W. and T. D. Epps. 1919-1920. The construction of thermocouples by electrodeposition. Proceedings of the Physical Society 32:326.

World Meteorological Organization, (WMO). 1963. Measurement of radiation and sunshine. In: Guide to meteorological instrument and observing practices. Geneva, Switz. p. IX 32.

Wyatt, Bruce. 1965. Unpublished data on surface water salinity, Newport hydrographic line. Corvallis, Oregon, Dept. of Oceanography, Oregon State University.

Wyrtki, Klaus. 1965. The average annual heat budget of the North Pacific Ocean and its relation to ocean circulation. Journal of the Geophysical Research 70(18):4547-4559.

# APPENDICES

# Appendix A: Voltage to Frequency Converter

## Parts List for Voltage to Frequency Converter

A. Resistors

R1, R2 - 2.0K, 1/2 watt, 5%
R3 - 1.0K potentiometer, 1/2 watt
R4, R5 - 3.9K, 1/2 watt, 5%
R6, R7, R19 -47 ohm, 1/2 watt, 5%
R8 - 2.2K, 1/2 watt, 5%
R9, R10 - 2.5K potentiometer. 1/5 watt
R11, R15 - 1.0K, 1/2 watt, 5%
R12 - 910 ohm, 1/2 watt, 5%
R13, R16 - 270 ohm, 1/2 watt, 5%
R14 - 270K, 1/2 watt, 10%
R17 - 33 ohm, 1/2 watt, 5%
R18 - 470 ohm, 1/2 watt, 10%

B. Capacitors

C1 - 4.0 μfd, 400 volt (Metal-film poly)
C2 - 6.0 μfd, 50 VDC (tantalum)

C. Transistors

Q1, Q2 - Fairchild, Matched pair in a single can, FSP-30
Q3 - 2N965
Q4 - 2N2646
Q5, Q7 - 2N1613
Q6 - 2N1306

D. Diodes

CR1, CR2 - 1N816
CR3 - 1N914

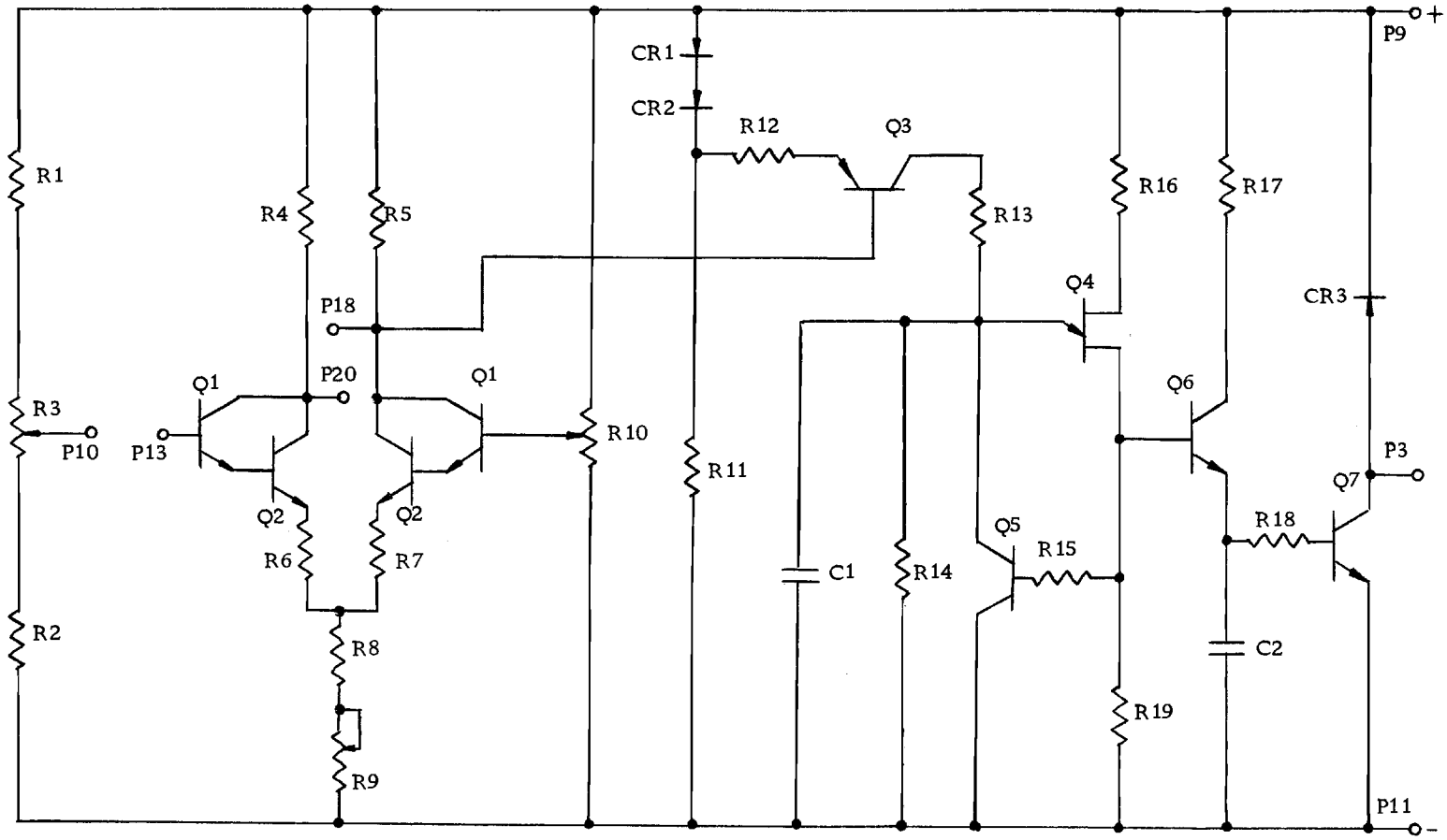


Figure 22. Voltage-to-frequency circuit diagram. Parts are listed on the preceeding page.

## Appendix B: Surface Water Temperature Buoy

Continuous measurements of surface water temperature were made with a specially designed buoy. Two precision thermistors (Yellow Springs Instrument Part No. 44005) were plotted into small plastic tubes and cemented into a depression on the underside of two of the three floats on the buoy (Figure 23). Each of the thermistors was capable of being switched into a Wheatstone bridge circuit similar to the bridge circuit described for measuring the transducer temperature. Calibration and balancing of the bridge circuit were done in a manner identical to that described for the transducer bridge circuit. Accuracies within ± 0. 3C are possible with the components described.

Three floats, constructed from hemispheres of polyfoam, were attached to a triangular frame of galvanized tubing and then filled with plastic foam. A steel rod bridle was attached to the triangular frame to hold the conducting cable. Displacements of less than 0. 75 inches were observed when the buoy was placed in the water with 40 feet of cable.

The temperature was recorded on the primary channel of a two channel strip chart recorder located in the lower chasis section of the data logging system (Figure 11).

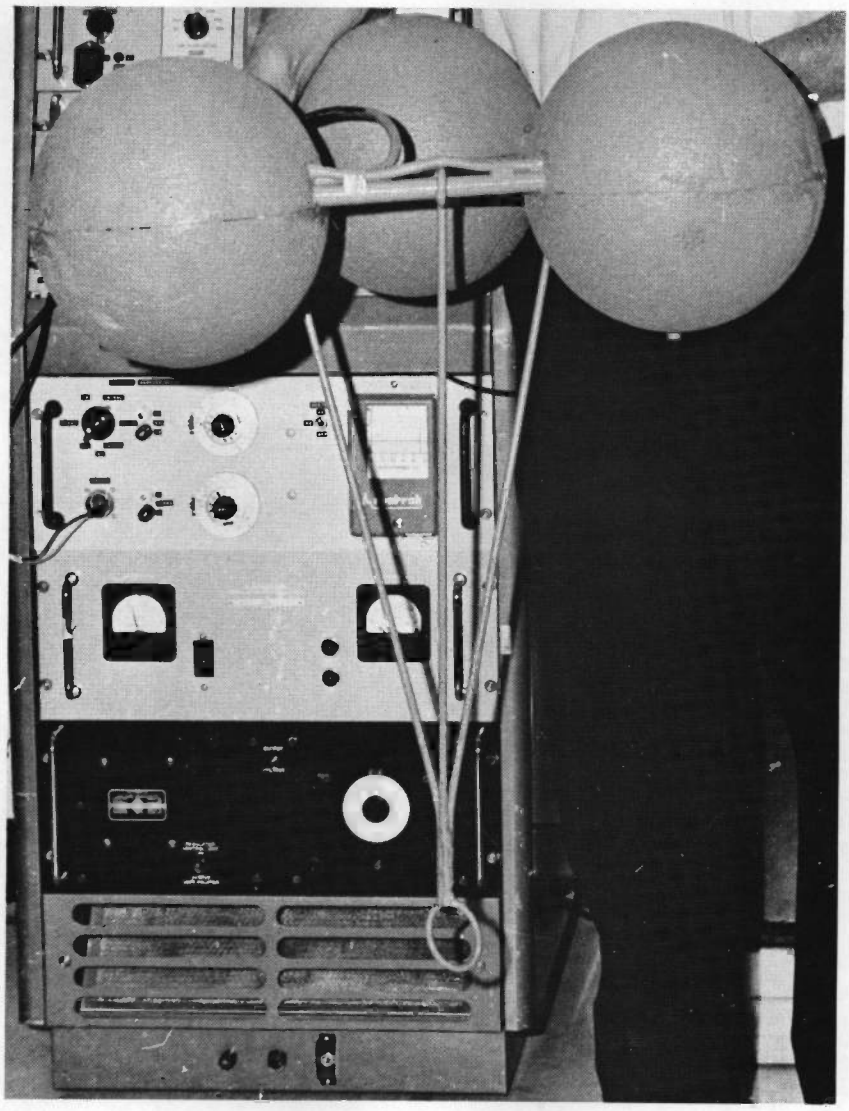

Figure 23. Buoy for measuring surface water temperature. In actual use, the buoy floats in the position shown. The two-channel strip chart recorder is shown behind the rod bridle of the buoy.